POLITECNICO DI TORINO

Master's Degree
in Civil Engineering

Master's Thesis

Predictive Maintenance: A Framework for Cable-Supported Bridges

Supervisor
Prof. Valerio De Biagi

Candidate
Lorenzo Casasso

March 2026

A nonno Gio e nonna Giulia

Summary

Predictive maintenance is an increasingly adopted approach for managing bridge upkeep, as it enhances long-term resilience, reduces lifecycle costs, and improves safety. This thesis aims to develop a predictive maintenance framework for suspension bridges that, drawing on degradation models available in the literature, enables the identification of optimal maintenance strategies in terms of both safety and cost-effectiveness.

First, aging models describing the loss of structural cross-section in bridge elements were examined. Then, two case studies were developed through detailed bridge modeling: one for a steel-deck bridge and another for a reinforced concrete–deck bridge. These case studies provided insight into the structural response to cross-section loss and supported the evaluation of different maintenance strategies to determine the most cost-effective solutions.

Contents

Chapter 1

Introduction

Over time, infrastructure undergoes a gradual decline in performance, particularly with respect to structural safety. This deterioration can result from several factors, including increasing traffic loads, fatigue phenomena, and the natural aging of materials. In this project, the focus is placed specifically on the degradation of structural materials.

Since the Industrial Revolution, the need to understand the mechanisms of material degradation has steadily increased. Early attention focused on iron, as corrosion in iron structures caused significant economic losses and motivated mid-19th-century studies on the effects of sea and river water, at various temperatures, on cast iron and wrought iron [1].

Throughout the years, construction techniques evolved alongside the materials employed, shifting from traditional stone to reinforced concrete, whose widespread adoption began in the 1930s. This transition prompted extensive research into concrete degradation mechanisms and the corrosion of steel reinforcement.

In recent years, Italy, like many other countries, has had to confront the condition of a large number of buildings constructed during the period of economic development following World War II. Many of these structures have exhibited significant deterioration in their structural materials. Focusing in particular on bridges, this degradation has resulted in several viaduct collapses, including some of national importance, such as the Morandi–Polcevera Bridge.

Following this major collapse, extensive inspections were carried out on bridges built during the same period. These assessments revealed that many had deteriorated to an unmanageable extent. Consequently, large-scale interventions were undertaken which, in several cases, due to the advanced state of deterioration,

ultimately required the complete reconstruction of the bridge.

Given the growing need for an in-depth understanding of material corrosion in infrastructure, particularly the need to study these phenomena over the entire lifespan of structures, it is essential to identify the causes of material deterioration and determine the actions that the authorities responsible for infrastructure management must take to preserve these assets and ensure user safety.

Moreover, it is not sufficient to understand material corrosion alone; a thorough knowledge of the structure and its structural behaviour is equally crucial. Without a clear understanding of how the structure responds, it becomes impossible to make informed decisions regarding the prioritization of interventions, the type of actions required, or the timeframe within which consolidation work must be carried out. These decisions have significant economic and logistical implications.

1.1 Goal of the project

As well established in the technical literature, different types of maintenance strategies exist. Reactive maintenance, or failure-based maintenance, is performed only after the performance level has fallen to the minimum acceptable threshold [2]. In contrast, predictive maintenance, implementable from the early stages of an infrastructure's life, is based on data analysis and continuous monitoring of degradable components to anticipate and identify imminent failures and to plan targeted interventions [3]. This approach relies on sensors and advanced technologies to collect information on the condition of structural elements. The acquired data is then analysed using complex mathematical models to predict when and where problems may arise, enabling timely and targeted actions.

Predictive maintenance offers the advantage of relatively low costs over the infrastructure's lifespan, as interventions are focused and help avoid unnecessary emergency repairs and associated downtime. Moreover, it enhances infrastructure reliability and safety by optimizing the use of available resources [4]. In addition to modern sensor systems, predictive maintenance can also be supported by procedures involving inspections, checks, and scheduled interventions aimed at preventing failures or malfunctions before they occur [5]. These activities are carried out when the structure exhibits specific vulnerabilities and are based on regular planning and periodic inspections of critical components [6].
The challenge, therefore, lies in identifying the points in a structure's lifespan at which inspections or maintenance interventions on a bridge become necessary. The central question of this project is how to effectively manage and understand the

behaviour of a bridge in relation to the corrosion of the materials from which it is constructed.

The aim of this thesis is to employ models developed in the academic literature to understand the degradation mechanisms affecting the materials used in bridges, with particular attention to reinforced concrete and steel. It also seeks to deepen the understanding of the behaviour of bridge structural elements, focusing especially on cable-supported bridges.

By integrating these two areas of study, it becomes possible to analyze how the behaviour of a bridge evolves as material corrosion progresses and structural resistance decreases. The subsequent step is to prevent the safety factor from falling below acceptable levels by establishing a maintenance management system capable of identifying the most advantageous solutions from both technical and economic perspectives. Ultimately, the objective is to provide a tool that supports the effective management of infrastructure under construction and, more broadly, the entire infrastructure network of a territory.

Chapter 2

Bridges: typologies and working principles

A bridge is a structure designed to provide passage across an obstacle without interrupting the obstacle itself. The types of passages it enables may include roads, railways, pedestrian routes, pipelines, or canals. The obstacles to be crossed can vary widely, such as rivers, roads, railways, or valleys. From an engineering perspective, bridges can be classified according to their geometry, for example as horizontal or sloping structures.

A typical bridge features a vertical axis perpendicular to the deck and its supporting piers. In a conventional configuration, the deck and supporting beams are arranged symmetrically with respect to the bridge's centerline, which coincides with its longitudinal axis. This configuration is considered ideal because it simplifies both structural analysis and construction, ultimately leading to a more economical design. For analytical purposes, the superstructure of a bridge is usually divided into smaller, more manageable components, such as girders, deck panels, barrier systems, joints, and diaphragms.

The design process begins by defining the requirements of the new bridge and the key characteristics of the site, which form the basis for all subsequent design decisions. Initially, the dimensions of the structural members are selected based on the designer's experience. At later stages, engineering software is used to compare alternative configurations and optimize member sizes. Finally, a complete structural analysis is performed for all critical construction phases, followed by the preparation of detailed shop drawings [7].

2.1 Historical background

The construction of bridges has always been driven by the need to overcome natural obstacles, such as valleys or rivers, by means of roads or footpaths, thereby facilitating travel, interaction between communities, and the exchange of goods and ideas. The evolution of bridges has accompanied human history, both reflecting and shaping the spirit of each era. For instance, the Romans were exceptional bridge builders, relying on fast and reliable connections to maintain and control their empire. After the fall of the Roman Empire, however, interest in bridge construction declined markedly until around the 9th century AD, as political entities became smaller and lacked the resources required to build and maintain such demanding structures.

Building a bridge has always represented a challenge against the forces of nature, accompanied by the constant risk of failure; yet it is precisely these difficulties that have fascinated people throughout history. The availability of new materials and the introduction of innovative technologies have revolutionized bridge design and construction, although the admiration inspired by ancient bridges that have survived to the present day remains comparable to that evoked by modern long-span structures.

Early bridges were constructed from natural fibers and resembled modern suspension bridges. The oldest known example of this type is a rope bridge over the Indus River near Swat, dating back to around 400 BC. However, suspension bridges were likely in use much earlier in regions such as Southeast Asia, South America, and Equatorial Africa.

Wood later became the primary material for bridge construction. Early beam bridges were formed from tree trunks placed across waterways. Wood was particularly suitable for this purpose because it can withstand both tensile and compressive stresses along the grain, and its light weight made it advantageous for spanning relatively long distances.
A remarkable advancement in bridge construction came with what is often considered the greatest invention of classical engineering in the field of tension: the arch. The arch made it possible to employ materials that are weak in tension, such as masonry, and it remained by far the most widely used bridge form until the mid-20th century.
In 1779, Abraham Darby III built the first cast-iron bridge over the River Severn in Coalbrookdale, England. Remarkably, in 1795 it withstood a major flood of the same river that destroyed many other bridges, demonstrating the superior strength of metal structures and encouraging their further development.

However, cast iron was relatively brittle and exhibited poor tensile strength, which eventually led to its replacement by steel. It is also worth noting that early metal bridges were still heavily influenced by traditional timber-construction techniques, with dovetail joints and mortise-and-tenon connections commonly employed.
The introduction of steel enabled progressively longer spans, supported by the evolution of structural systems: from simply supported beams to continuous beams, from solid girders to trusses, from inclined or arched pier systems, and ultimately to suspension bridges.

In 1867, a French gardener named Joseph Monier obtained a patent for the construction of cement pots and containers reinforced with iron, marking the birth of reinforced concrete, which would become widely used in the twentieth century. Reinforced concrete relies on the effective collaboration between concrete, which resists compressive stresses and provides rigidity to structural elements, and steel, which resists tensile stresses. This new material revolutionized the construction industry: it enabled the creation of virtually any shape and proved highly competitive from an economic standpoint.

In bridge construction, reinforced concrete was initially applied to traditional forms typical of masonry bridges, without fully exploiting its potential. Over time, however, it began to be used more freely, unconstrained by these traditional shapes, allowing for entirely new structural forms. Although reinforced concrete cannot match steel in terms of achievable span length, it offers significant advantages in durability and versatility [8].

2.2 The major parts of bridges

Every bridge can be divided broadly into three parts [9]:

- Superstructure. The part of the structure that supports traffic and includes deck, slab and girders. All the parts of the bridge which are mounted on a supporting system can be classified as a superstructure

- Substructure. The part of the structure, i.e. piers and abutments, which supports the superstructure and which transfers the structural load to the foundations.

- Foundation. It is the component which transfers loads from the substructure to the bearing strata. Depending on the geotechnical properties of the bearing strata, shallow or deep foundations are adopted. Usually, piles and well foundations are adopted for bridge foundations.

In particular, since this thesis does not focus on the detailed study of bridges themselves but rather on their macro-structural behaviour, attention will be directed to the most significant components of the structure [10]:

- Abutment. A substructure element supporting each end of a single span or the extreme ends of a multi-span superstructures and, in general retaining or supporting the approach embankment;

- Deck. The roadway portion of a bridge that directly supports vehicular and pedestrian traffic and transfers this load to the supports. There are many types of deck, made of precast element or cast in place element and in relation of shape could be used box element (Figure 2.1) or beams element;

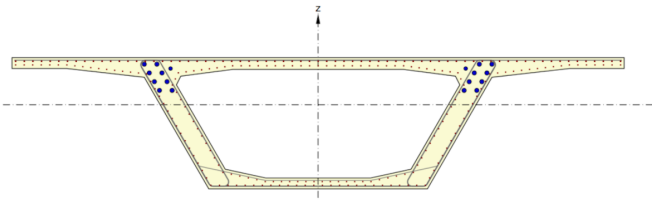

Figure 2.1. Box girder bridge section

- Bearing. Devices installed between bridge substructure and superstructure to transfer the applied vertical and horizontal loads. In addition they allow relative movements between superstructure and substructure, for instance, rotation movements and translational movements in longitudinal and transverse direction;

- Pier. An intermediate supports of the bridge superstructure; transfer the loads to the foundation;

- Foundation. Structural element in direct contact with the soil which transfer the loads from the structure to the soil. Generally the foundations can be classified in two types, namely shallow foundations and deep foundations;

In this thesis, the only parts studied were the deck and cables of the suspension bridge.

2.3 Classification of bridges

Bridges can be classified according to various criteria, such as the type of obstacle they must cross. In this study, however, they will be considered in terms of their structural system and the materials used.

2.3.1 Girder Bridges

Girder bridges consist of one or more girders, linear, nearly horizontal elements, straight or curved in plan (Figure 2.2), that carry gravitational loads along the longitudinal direction of the bridge, i.e., along the bridge axis, primarily through vertical shear and longitudinal bending. These girders are supported by the substructure, which includes the abutments at the bridge ends and piers that provide intermediate support along the bridge's length.
Vertical shear forces and longitudinal bending moments are not the only forces acting on a girder bridge, but they usually dominate over other forces, particularly torsion. Strictly speaking, any bridge in which normal forces in the girders are caused by gravitational loads is a frame bridge rather than a girder bridge. However, bridges in which normal forces under gravitational loads are minor, such as those caused by monolithically connected piers, are still commonly referred to as girder bridges.

In girder bridges, including the bridge deck, constitute the superstructure. In other types of bridges, such as arch or cable-stayed bridges, the superstructure includes additional elements that provide support to the bridge girders and ensure the overall longitudinal transfer of gravitational loads, either entirely or in combination with the girders. The behaviour of the bridge girder is analogous to that of the superstructure in a girder bridge, regardless of the bridge type.

The main function of the bridge deck is to carry traffic loads, as well as its own weight and superimposed dead loads, including surfacing, waterproofing, and guardrails, and to transfer these loads to the longitudinal girders. In doing so, the deck acts as a slab, typically carrying loads primarily in the transverse direction.
In steel–concrete composite bridges (Figure 2.2), transverse girders (cross-beams), usually composite with the concrete deck, may be used to support the deck and carry loads in the transverse direction. When the spacing of the cross-beams is small relative to the separation of the longitudinal girders, the concrete slab primarily carries loads in the longitudinal direction. In such cases, either the concrete slab alone or the slab together with the cross-beams is considered the deck; these configurations are also referred to as ladder deck bridges.
In an efficient cross-section, the deck contributes significantly to the longitudinal

stiffness of the girder, acting as the top flange in standard bridges or as the bottom flange in trough bridges. To activate the deck slab, the connection between the longitudinal girders and the deck must be able to transfer the required longitudinal shear forces. In steel–concrete composite bridges, shear connectors are provided for this purpose.

It should be noted that in older railway bridges without a ballast trough, and in early bridges with a concrete deck on steel girders, the deck was intentionally separated from the girders so that it did not contribute to the overall longitudinal load transfer. Similar solutions may be necessary to allow the deck to be replaced without affecting the other parts of the bridge, thereby ensuring repairability and circularity. However, this approach is structurally inefficient. Beyond its structural role, the deck must incorporate all elements required to ensure the functionality of the roadway, railway, or pedestrian path it supports, including surfacing or ballast for road and railway bridges, respectively, as well as drainage systems, noise protection, guardrails, and handrails.

Concrete decks are the standard solution for road and railway bridges because

Figure 2.2. Construction of a Girder Bridge [11]

they are economical and robust. When properly waterproofed, they are also highly durable. Additionally, fatigue is generally a minor concern for concrete decks. On the other hand, concrete decks are relatively thick and heavy, which may necessitate alternative solutions when self-weight or clearance requirements are critical.

Orthotropic steel decks are commonly used in long-span bridges because they are significantly lighter than concrete decks. They are also thinner, thanks to the

use of stiffeners placed within the same depth as the longitudinal girders, making them an effective solution when clearance requirements are critical, that is, when the total depth of the bridge girder from soffit to surfacing must be minimized. The durability of orthotropic steel decks depends heavily on the quality of waterproofing, even more so than in concrete decks [12].

2.3.2 Arch Bridges

An arch is a curved structure that supports loads along its axis of symmetry, and a bridge that uses an arch as its primary load-carrying system is called an arch bridge. An arch bridge is typically defined as a vertically curved, axially compressed structural member that spans an opening and provides support for the moving loads above it. The structural behaviour of an arch depends on its shape and the number of hinges (Figure 2.3). In general, arches become stronger as the number of hinges decreases; however, this also significantly affects settlements. Arch bridges can be constructed as single-span structures with two abutments or as a series of continuous arches. Arch bridges have been widely used worldwide due to their distinctive aesthetics and are commonly employed for long spans, following suspension and cable-stayed bridges.

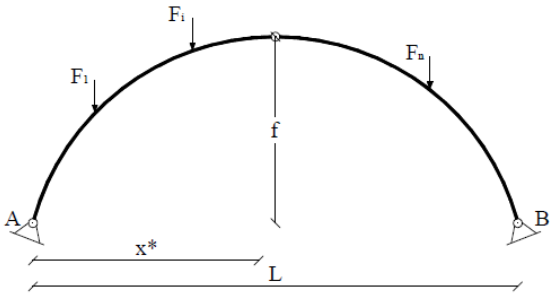

Figure 2.3. Three hinge arch scheme

There are many different types of arch bridges, but they all share some fundamental elements. Each bridge includes abutments that support the curved arch structure. As the name suggests, the bridge incorporates an arch shape. Loads are transferred along the curve of the arch toward the supports rather than acting directly downward, which prevents excessive pressure from concentrating on any single part of the structure. When properly designed, the arch, which carries the majority of the load, is subjected primarily to compression. For this reason, arch structures were widely used in ancient times with stone materials. The properties of concrete, weak in tension but strong in compression (Figure 2.4), make it particularly well suited for arch bridges. This is a significant advantage, especially

considering the issues of cracking and corrosion that affect reinforced concrete bars.

In 1875, the first reinforced concrete arch bridge, the Marquis of Tilière de Chazelet, was designed by Monier. With the rapid expansion of railway and canal networks in the first half of the twentieth century, many bridges were constructed, particularly in Europe. Most short and medium-span bridges were masonry arch bridges, while very few long-span masonry arches were built, as they could not compete with new materials such as iron, steel, and concrete. During the twentieth century, concrete arch bridges became increasingly common. In 1904, Hennebique built the Risorgimento Bridge in Rome, featuring a span of over 100 meters. The development of concrete arch bridges also contributed to advancements in steel arch bridge applications [13].

As noted, reinforced concrete bridges have been widely developed, but reinforced concrete is also used in combination with steel truss elements for the arch itself. Furthermore, the elements connecting the deck to the arch may carry loads either in tension, using steel cables (suspenders), or in compression, using reinforced concrete struts or piers. Similar to girder bridges, the decks of arch bridges may be constructed from reinforced concrete or designed as composite (mixed) decks.

Figure 2.4. Arch Bridge

2.3.3 Truss

In the past, some people considered the truss bridge as a distinct type of bridge; however, it is more accurately described as a combination of different structural members. Truss bridges primarily use a truss framework in which all members are hinged together, forming multiple triangles. Triangles are well-known for being the most stable shape in a 2-D structure. In a truss bridge, shear forces do not act directly on the members; instead, the structure transfers shear, stress, and bending moments, common in other types of bridges, into simple axial tension and compression forces (Figure 2.5). Because of this efficient structural system, truss bridges can withstand greater tension and compression compared to other bridge types of the same span, resulting in higher bending strength. Additionally, for bridges of the same length, truss bridges often use less material.

The evolution of truss bridges has involved changes in both structure and materials, as well as the integration of smart technologies, such as monitoring instruments that track structural parameters. These systems provide information on fatigue and degradation, simplifying maintenance and inspection procedures for engineers.

Over time, the focus of truss bridge development has gradually shifted from purely improving safety to enhancing pedestrian convenience and facilitating maintenance. This approach extends the service life of the bridge and allows building materials to be used more effectively. The first truss structures can be traced back to the 16th century, when the Italian architect Palladio developed early designs. Subsequently, bridges in Europe and the USA evolved from simple triangular forms to more complex truss configurations, and eventually returned to simplified triangular structures. Bridges that have withstood the test of time continue to survive today.

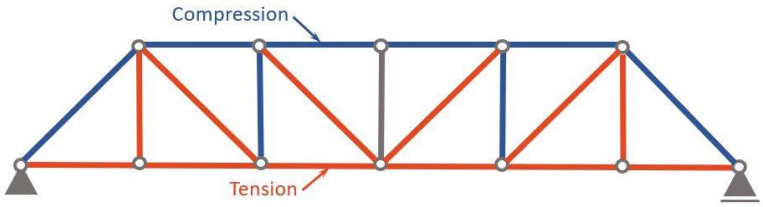

Figure 2.5. Static scheme of a truss bridge

In recent years, researchers have been exploring the use of new materials for various types of structures. In the case of truss bridges (Figure 2.6), innovations such as steel-tube truss bridges and steel–concrete composite truss bridges have been studied. These designs combine the advantages of both steel and concrete

bridges. Compared with conventional steel truss bridges, these hybrid trusses offer greater stiffness. In addition, construction debris can be recycled and incorporated into the building process of other structures. Given the continued importance of railway transportation, using this type of structure can reduce costs and extend the service life of the bridge.

In conclusion, the development of truss bridges has a long history, with materials gradually evolving from timber to steel. In recent years, scientists and engineers continue to explore new materials and structural designs to increase load-bearing capacity while minimizing costs [14].

Figure 2.6. A truss bridge converted to pedestrian use and pipeline support [15]

2.3.4 Cable-supported Bridges

It was decided to include, two types of bridges in the same subchapter because they use the same structural macro elements: piers, decks and cables.

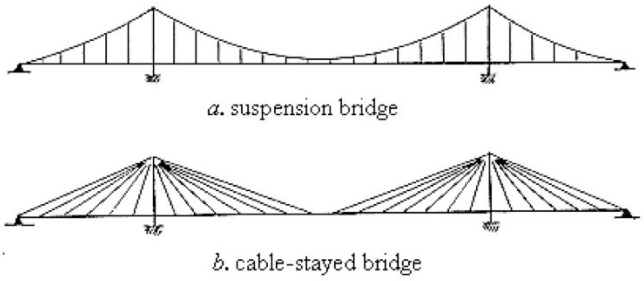

Figure 2.7. Suspension bridge and Cable-stayed bridge

Cable-Stayed Bridges

A cable-stayed bridge consists of a deck, towers, and cable-stays (Figure 2.8). The deck is supported along its entire length by a number of inclined stays. These bridges enable large-span structures with relatively shallow decks, functioning essentially as a series of beams. Towers transfer compressive forces to the foundations, while the cable-stays convey vertical deck loads to the towers.

The behaviour of cable-stayed bridges is highly sensitive to the distribution of cable forces and the stiffness of the load-carrying components. Their narrow decks and distinctive cable layouts offer aesthetic appeal and make them an effective structural solution for medium-to-long spans. Lightweight, flexible, and low-damping stay cables are critical components, but they are constantly subjected to dynamic stresses, which can lead to fatigue and fracture.

Various measures, such as cross-ties, surface profiling, and structural vibration control mechanisms, are employed to enhance performance under dynamic loads. Cable-stayed bridges play a key role in transportation infrastructure, and ensuring their structural integrity and functionality is essential. Regular inspection of the cables is crucial for safety, as they carry both live and dead loads to the towers. Over time, external factors such as fatigue, vibrations, and galvanic corrosion can degrade the cables, reducing load capacity and potentially affecting the strain distribution and alignment of the structure. Temperature variations can also induce parametric changes, leading to inaccuracies in estimating mass, damping, and stiffness. Adaptive control techniques are a viable solution, offering robustness in managing these fluctuations.

The typical structural designs of cable-stayed bridges can be divided into two basic categories, which differ primarily in terms of their static behaviour, while their formal distinction is determined only by the geometric arrangement of the stays, which may be harp-shaped or fan-shaped [16].

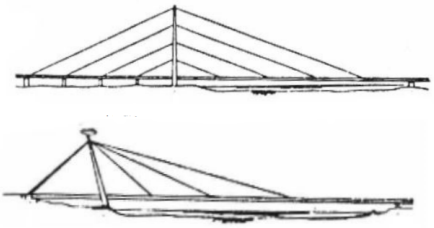

Figure 2.8. Harp-shaped and fan-shaped cable-stayed bridges

From a static point of view, if we compare the two type of cable-stayed bridges, with identical geometric characteristics, the harp-shaped (Figure 2.10) configuration induces normal stresses in the deck that are approximately twice those of the fan-shaped bridge (Figure 2.9).

If we assume that the spacing (Δ) between the stays is very small, and considering the fan-shaped configuration, we obtain:

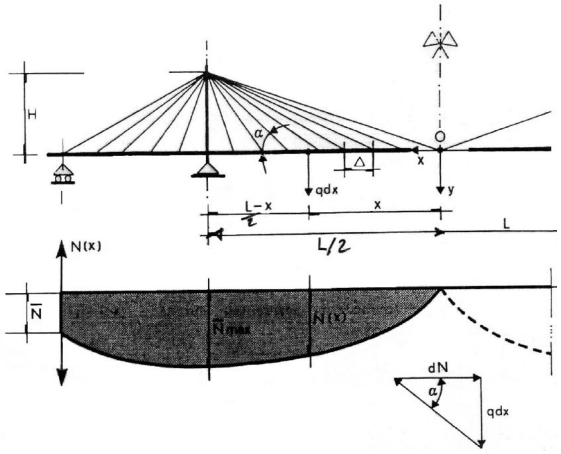

Figure 2.9. Normal stress in the deck with Fan-shaped arrangement

$$\frac{qdx}{dN} = tan\alpha = \frac{H}{L-x} \tag{2.1}$$

We can calculate the maximum normal stress by solving the equation for N and integrating between 0 and L.

$$N_{max}(x = L) = \frac{qL^2}{2H} \tag{2.2}$$

The same thing can be done for the harp-shape:

$$\frac{qdx}{dN} = tan\alpha = \frac{H}{L} \tag{2.3}$$

Explicitly N and integrating again between 0 and L:

$$N_{max}(x = L) = \frac{qL^2}{H} \tag{2.4}$$

Considering the same normal stress in the deck, the harp arrangement requires tower heights twice those of the fan configuration. Although the harp pattern is

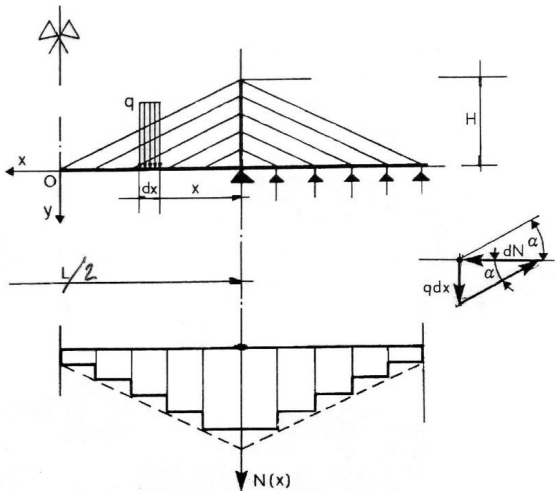

Figure 2.10. Normal stress in the deck with Harp-shaped arrangement

not optimal from either a static or economic standpoint, it remains appealing due to its undeniable aesthetic advantages.

Furthermore, the arrangement of the supports, and therefore the structural static scheme, can vary depending on the type of deck. If the deck is made of concrete, the objective is to keep it in compression, whereas if the deck is made of steel, the aim is to keep it in tension in order to prevent buckling of the beam.

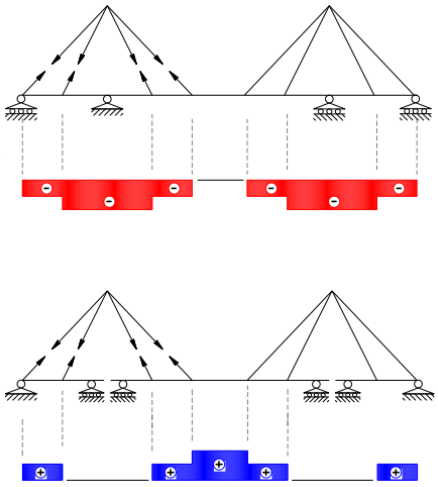

Figure 2.11. Different configuration of supports in a Cable-stayed bridge

In the Figure 2.11 it can be observed that the presence or absence of a support at the piers leads to a change in the stress state of the deck, which is a key factor in selecting the appropriate material. In particular, when a support is provided at the piers, the deck is predominantly in compression, making concrete a suitable choice. Conversely, when no support is present, the deck is mainly subjected to tension, for which steel is the more appropriate material.

Suspension Bridges

The suspension bridge (Figure 2.13) is defined by a main structural system consisting of cables with very low flexural stiffness, which support the deck through a series of vertical hangers. This configuration enables the construction of bridges with very long spans, and for this reason suspension bridges are currently used almost exclusively for large-span applications. Historically, suspension bridges were employed primarily for lightweight pedestrian crossings; however, advances in materials, aerodynamics, and structural analysis now allow them to carry highway traffic and even railway loads.

The statics of this structural system (Figure 2.12) are relatively straightforward: the weight of the deck is transferred to the vertical tension members, known as hangers, which in turn convey the loads to the main cables. These cables pass over the towers, subjecting them primarily to compressive forces, and are finally anchored to massive anchor blocks embedded in the ground. However, the global behaviour of the structure becomes more complex due to the delicate equilibrium configuration of the main cables. Owing to their negligible flexural stiffness, these cables deform significantly under load, and their geometry changes with every variation in the applied loads. This geometric nonlinearity is a key aspect in the analysis and design of suspension bridges.

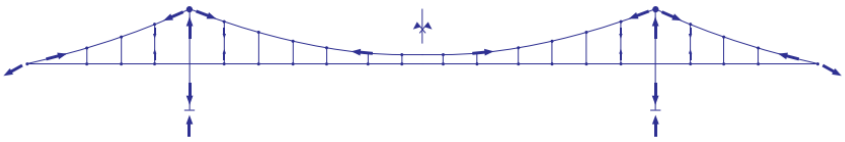

Figure 2.12. Suspension Bridge static scheme [17]

The main cables are the main elements of the structure. These consist of numerous steel wires, which are then compressed together to form a single cable. The vertical stays are also made of steel in modern bridge construction, but they have a much smaller diameter than the main cables. Their task is to support part of the deck, which depends on the distance between them. The towers are generally the

most imposing element of the bridge, as they must support the load of the deck, which is transmitted to them by the cable. Furthermore, for a suspension bridge with a large span, the deck must be designed in a particular way. It must have high torsional strength to ensure good stability and resistance to the horizontal forces of the wind.

Suspension bridges and similar structures are susceptible to flutter, a fluctuating aerodynamic response. As demonstrated by the collapse of the Tacoma Narrows Bridge, flutter can lead to structural failure. To improve flutter performance, barriers and streamlined box-girder designs have been optimized. However, laboratory testing is still commonly used to evaluate flutter behaviour, and assessing structural vibrations is essential for both flutter research and failure analysis.

They offer several advantages, including reduced main cable tension, smaller anchoring requirements, longer possible span lengths, and overall cost efficiency. The main cable, composed of high-strength steel, is critical to the bridge's performance and design lifespan, making its integrity essential for extending the bridge's service life.

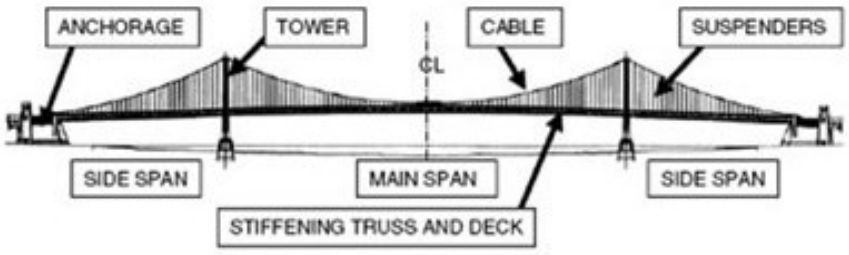

Figure 2.13. Suspension bridge

They are exposed to significant corrosion risks from environmental pollutants such as, dust, sulfides, and chlorides. Over a decade of research has focused on preventing corrosion in suspension cables and other components. Atmospheric corrosion accounts for more than half of the corrosion loss in these structures. Modern railroad suspension bridges with primary spans exceeding 1,000 meters often incorporate flexible nanocomposite materials. Truss-girder structures are used to enhance girder rigidity while meeting safety requirements for high-speed trains.

Due to daily temperature variations and solar radiation, the high thermal conductivity and linear expansion of steel can produce non-uniform temperature fields.

Trusses, being highly statically indeterminate structures, generate secondary internal forces when subjected to these temperature fluctuations [18].

In short, a suspension bridge is based on simple techniques that have been used for centuries, but as the span increases, so do the difficulties, starting with the study of corrosion of the structural elements that compose it.

Chapter 3

Ageing in structural materials

The study of corrosion in construction materials is of fundamental importance for ensuring the durability and safety of structures. Corrosion is one of the primary causes of material degradation in the built environment, as it progressively reduces performance, shortens service life, and increases maintenance and repair costs.

Understanding corrosion mechanisms is therefore essential for anticipating the progression of damage, designing more durable materials, and implementing effective prevention and mitigation strategies. By examining the physical, chemical, and mechanical interactions that govern degradation, it becomes possible not only to protect structures more effectively but also to ensure their long-term sustainability from both safety and economic perspectives.

The deterioration of materials in bridges is a critical issue that affects all types of construction materials. In this thesis, the analysis is limited to two specific materials: reinforced concrete and carbon steel.

3.1 Reinforced Concrete

Concrete is a mixture of binder (cement), mixing water (added water), and aggregates (inert particles). Once mixed with water, the cement begins to react chemically. As a result of cement hydration, two new mineral substances are formed:

- Small needle-like formations of calcium silicate hydrates (CSH) with slightly variable composition, which intertwine to form a compact and very hard

structure;

- Large flat crystals of calcium hydroxide ($Ca(OH)_2$), which do not contribute to the hardness of the material but, due to their strong alkaline nature, help protect the reinforcement from corrosion.

This process, known as cement hydration, involves a significant release of heat, referred to as hydration heat, and ultimately leads to the setting and progressive hardening of the cement paste [19].

The durability of reinforced concrete structures is strongly influenced by degradation phenomena affecting both the cementitious matrix and the steel reinforcement. These mechanisms, which may be physical, chemical, or mechanical in nature, can primarily affect either the concrete or the steel; however, they inevitably produce reciprocal effects, creating a strong interaction between the two components.

A key factor is the porosity of the cementitious matrix, which governs its permeability to external agents and largely determines the severity of deterioration. Higher porosity facilitates the ingress of water, oxygen, and aggressive substances, thereby accelerating corrosion processes that compromise the stability and safety of the structure (Figure 3.1).

Figure 3.1. Concrete degradation in a bridge deck [20]

The main mechanisms of degradation in reinforced concrete are listed below [21]:

- **Washout**. The first phenomenon to consider is washout, which refers to the loss of binding material due to the action of a solvent liquid. Portlandite is particularly susceptible to this process when exposed to pure water. Since it is the most abundant crystalline compound in cement paste, its dissolution leads to a significant reduction in the material's mechanical properties.

If the water were stationary, the phenomenon would tend to slow down as it progressed, eventually reaching a concentration equal to the solubility limit in water. However, if the water is moving, the process may theoretically continue until all available $Ca(OH)_2$ has been dissolved.

Flow velocity therefore plays a crucial role. Figure 3.2 shows a schematic representation of the leaching rate of lime (CaO) in concrete. Between points a and b, the water flow is relatively slow, and the pore water remains saturated with lime. Over time, or if the water flow increases, the pore walls become depleted of solid lime. When this occurs, the concentration of lime in the water decreases, as indicated at point b. In the segment $c-d$, the leaching rate is governed entirely by the diffusion of $Ca(OH)_2$ from the interior of the material toward the flow paths.

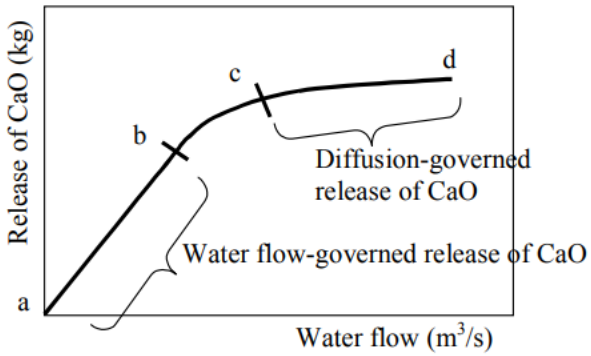

Figure 3.2. Release of portlandite as a function of water flow in contact [22]

- **Acid attack**. Given the basicity of most phases present in concrete, these compounds act as proton acceptors and are therefore particularly susceptible to acid attack. Such attacks cause significant concrete washout, with a rate that depends on both the specific hydration product involved and the type of acid present. Common aggressive acids include sulfuric acid, hydrochloric acid, nitric acid (which may form through the conversion of vehicle-emitted NO_x in acid rain), and carbonic acid.

  The phenomenon also affects silicate phases, leading to their decalcification; however, it is far more pronounced and rapid in the case of portlandite. For this compound, the fundamental reaction can be expressed as follows:

$$Ca(OH)_2 + acid \longrightarrow acidsalt + H_2O \tag{3.1}$$

The aggressiveness of an acid depends largely on the solubility of the salt produced during the reaction: the more soluble the resulting salt, the more severe the attack. For this reason, hydrochloric acid is considered more aggressive than phosphoric acid or most organic acids.

- **Sulphate attack**. It is useful to make a preliminary distinction between: the external sulphate attack, where sulphate ions penetrate the concrete through the action of aggressive water; and the internal sulphate attack, where sulphates are present in the aggregates or cement clinker (it should be noted in this regard that dihydrate or semi-hydrate gypsum and anhydrite are added specifically as setting regulators).

  The sulphate ion SO_4^{2-} is capable of reacting with calcium hydroxide $Ca(OH)_2$ to form gypsum according to the reaction:

$$Ca(OH)_2 + SO_4^{2-} + 2H_2O \longrightarrow CaSO_4 \cdot 2H_2O + 2(OH)^- \tag{3.2}$$

  As a result, the gypsum content increases, resulting in an excess compared to the quantity expected in the clinker and causing, through an expansive reaction with the hydrated calcium aluminates C-A-H, the formation of secondary ettringite and the consequent detachment of the external parts of the product.

- **Alkali-aggregate reactions**. These phenomena primarily cause long-term damage due to internal expansion and the resulting cracking. The kinetics of these reactions are highly dependent on environmental conditions and the concrete mix. However, for these reactions to be initiated and sustained, several conditions must occur simultaneously. First, the aggregates must be reactive; in this regard, a higher quartz crystal content increases reactivity, and the same effect is observed when particle size decreases, as this leads to a larger specific surface area.

  In addition, the interstitial fluid must exhibit high basicity, mainly determined by the presence of OH^-, Na^+, and K^+ ions. Finally, sufficient moisture is required; for alkali–silica reactions, a relative humidity of approximately 80–85 % is necessary. It has also been observed that the presence of calcium promotes the reaction, which is consistent with the lower susceptibility of pozzolanic cements to this type of degradation.

- **Carbonation**. This mechanism causes a decrease in pH, which leads to the breakdown of the passivation film previously established in the interstitial alkaline solution, where a pH greater than 11.5 ensures a substantial inhibition of anodic steel dissolution. When the pH falls below this threshold, the passive layer becomes unstable and eventually breaks down.

- **Corrosion of rebars**. Corrosion of reinforcement is a process that develops within reinforced concrete when the passivation film breaks down. This leads to an increase in the volume of the steel bars, which in turn causes cracking and a reduction in the effective concrete cross-section.

Analysing all the causes of concrete degradation would be complex in a preventive assessment, as they depend on numerous interacting factors. For this reason, the present thesis focuses on a selected set of degradation mechanisms. Specifically, it will first examine carbonation and chloride attack, both of which lead to the breakdown of the passivation layer that protects the reinforcement. It will then analyse reinforcement corrosion itself, the stage at which part of the structural capacity is lost. Finally, it will investigate the detachment of the concrete cover caused by bar corrosion and the associated volumetric expansion due to rust formation. The life cycle of the concrete structure described in [23] is shown in Figure 3.3.

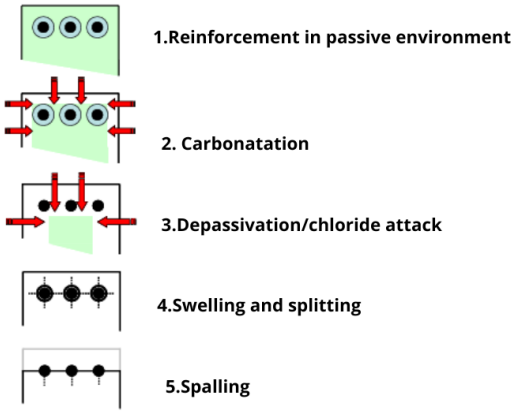

Figure 3.3. Time evolution of structural degradation (carbonation and chloride attack)

3.1.1 Carbonation

Concrete usually contains numerous pores and microcracks, invisible to the naked eye, both on the surface and inside the material. Carbon dioxide (CO_2) from the air can penetrate the concrete through these pores and cracks. Concrete also contains alkaline substances, such as $Ca(OH)_2$. When CO2 and $Ca(OH)_2$ come into contact over time, a slow chemical reaction occurs, consuming $Ca(OH)_2$ aand producing calcium carbonate ($CaCO_3$) and water. As a result, carbonation reduces the alkalinity of concrete. When carbonation reaches beyond the protective layer

of concrete, it compromises the protection of the steel reinforcement, which begins to corrode in the presence of water and air. Therefore, carbonation shortens the service life of concrete structures. Studying and predicting carbonation depth is of great significance for evaluating the remaining life of concrete structures and for planning necessary maintenance measures.

Mathematical curve models are widely used for predicting carbonation depth and chloride ion penetration. These models offer two main advantages: each parameter has a clear physical meaning, and only a small amount of experimental data is required for curve fitting, making the calculations relatively simple.

The earliest mathematical model for predicting carbonation depth is based on Fick's Law, shown in Equation [3.3] as:

$$x = \alpha\sqrt{t} \tag{3.3}$$

where x denotes the depth of carbonation in concrete, t denotes the carbonation time, and α is the carbonation coefficient that reflects the rate of concrete carbonation in a comprehensive manner. Fick's Law states that the carbonation depth of concrete is proportional to the square root of carbonation time. The advantage of the model in Equation 3.3 is that it contains only a single unknown parameter, the carbonation coefficient, making it very convenient to apply. However, the limitation of this model is that it is difficult to account for the influence of multiple factors on the carbonation depth of concrete. To overcome this limitation, many new mathematical models have been developed that consider various factors such as temperature, relative humidity, CO_2 concentration, aggregate type, curing time, and external loads. By integrating these factors, the accuracy of Fick's Law can be improved.

In [24], several mathematical models are analyzed, but this document reports only three that are suitable in practice. Equation 3.4 [25] is mainly suitable for recycled aggregate concrete, and in this model all the adopted coefficients are theoretical values, which may deviate from the true values.

$$x = m \cdot k_A \cdot \sqrt[4]{T} \cdot k_e \cdot \sqrt{\frac{k_c \cdot W}{f_c^3 \cdot C}} \cdot k_{CO_2} \cdot \sqrt{t} \tag{3.4}$$

where:
k_A : the water absorption rate of the aggregate;
T : temperature;
$k_e = RH^{1.5}(1 - RH)$,where RH represents relative humidity;
k_c : the execution transfer parameter;

f_c : the 28 day compressive strength (MPa);
W : the water content;
W : the cement content;
k_{CO_2} : the concentration of CO_2 ;
m : a constant parameter.

The Equation 3.5 [26] optimizes Fick's law, but is mainly suitable for recycled aggregate concrete and mainly considers the effect of equivalent water absorption of aggregate mixture (EWA) on carbonation.

$$x = K_c \cdot \sqrt{t} = (72.470 - 0.772 f_c - 0.117 C_0 + 4.617 c + 1.594 EWA) \cdot \sqrt{t} \quad (3.5)$$

where:
C_0 : the clinker content (kg/m^3);
c : the content CO_2 (%);
EWA = the equivalent water absorption rate of aggregate mixture (%).

The Equation 3.6 [27] relies too much on the accuracy of water–cement ratio. On the other hand, this approach can be very useful when limited information is available. It can be applied to new structures, as the water-to-cement ratio is determined during the design phase. For existing structures, a petrographic analysis can be performed on samples from the bridge to determine the ratio.

$$x = -0.56213 - \frac{8.792}{\sqrt{t}} + 17.8372(w/c) \quad (3.6)$$

where:
w/c : the water-cement ratio of concrete.

Considering these mathematical methods, and taking into account the structure, the materials used, and the environment, we can calculate the depth of carbonation over time. In particular, by knowing the thickness of the concrete cover, it is possible to quickly estimate the time required for complete depassivation of the cover and, consequently, the onset of corrosion of the reinforcement bars.

It is important to emphasise that the models described were developed under specific environmental conditions, and in most cases these conditions do not perfectly correspond to those of the structure being analysed. As a result, the predictions obtained from these models do not exactly reflect the actual degradation experienced by the structure. Moreover, the models themselves contain inherent uncertainties,

arising from various influencing factors. For this reason, a large number of simulations must be performed in order to obtain a range of values within which the actual behaviour is likely to fall.

If chlorides are present in the environment, they can contribute to the breakdown of the reinforcement's protective layer. It is therefore necessary to evaluate the time required for chlorides to diffuse from the exterior into the concrete until they reach a critical concentration capable of destroying the passive oxide film. If this time is shorter than the time required for carbonation to reach the reinforcement depth, the initiation period will be governed by chloride attack.

3.1.2 Chloride attack

Diffusion is a chemical process that tends to equalize the concentration of a chemical species within a medium. The laws governing this phenomenon are mathematical relationships that have been known since the second half of the 19th century, when Adolf Fick formulated the principles that now bear his name. These laws were established by observing how a mass of diffusing substance (such as salt) disperses into a solvent (such as water) across a defined interface. They are phenomenological in nature, meaning they were derived solely from empirical observations of the physical process, without reference to more fundamental laws. Numerous experimental studies conducted since then have confirmed both their effectiveness and their limitations. The models used to describe chloride diffusion in concrete are based on these principles [23].

Fick's second law was first applied to chloride penetration in concrete by Collepardi in 1970. During the 1990s, the model was further refined, and MC 90 provided an expression for evaluating the chloride concentration at a depth x, as reported in Equation 3.10.

$$C(x,t) = C_0 + (C_{s,\Delta x} - C_0) \cdot [1 - erf(\frac{x - \Delta x}{2 \cdot \sqrt{D_{app}(t) \cdot t}}] \tag{3.7}$$

Δx represents the depth of the replacement surface (Figure 3.4). In the presence of a spray zone, Fick's law cannot be considered valid because other, much faster transport mechanisms, such as capillary suction, dominate the process. For practical purposes, this replacement depth can be assumed to range between 6 and 11 mm for concrete located within approximately 1.5 m of street level. The Gaussian error function, $erf()$, is described by the integral in Equation 3.8:

$$erf(x) = \frac{2}{\sqrt{\pi}} \cdot \int_0^z -e^{-\eta^2} \tag{3.8}$$

Estimates of the Equation 3.8 are available in the literature and avoid the calculation of the integral. A good approximation is provided, by the expression 3.9:

$$erf(x) = \frac{1}{(1 + 0.278393z + 0.230389z^2 + 0.000972z^3 + 0.078108z^4)^4} \tag{3.9}$$

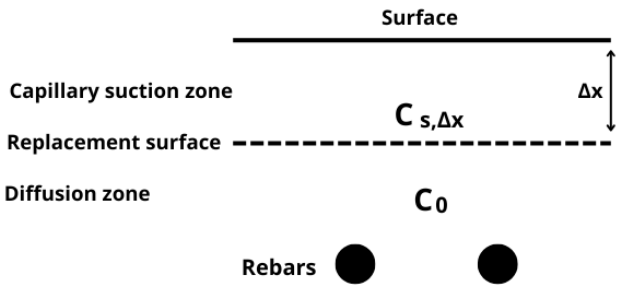

Figure 3.4. Concept of diffusion surface.

In Equation 3.10, C_0 is the initial chloride content of the concrete (% by weight of cement), and $C_{s,\Delta x}$ indicates the chloride content at the exposed surface. The values of these concentrations can be found in MC 90 [28] for specific types of environments; for the evaluation of C_0, analyses of the construction materials are necessary. Given the large number of environmental conditions presented in MC 90, they will not be reproduced here; instead, some reference values are provided as examples. The apparent diffusion coefficient, $D_{app}(t)$ [29], is evaluated as:

$$D_{app}(t) = k_e \cdot D_{RCM,0} \cdot k_t \cdot A(t) \tag{3.10}$$

where:
k_e and k_t could be set as 1;
$D_{RCM,0}$ is the chloride migration coefficient (m^2/s), this parameter change in relation to the $\frac{w}{c}$ and the type of cement [30].

The function $A(t)$ is related to the ageing of concrete:

$$A(t) = (\frac{t_0}{t})^a \tag{3.11}$$

Type of Cement	Minimum Value $[m^2/s]$	Maximum Value $[m^2/s]$
CEM I	$8 \cdot 10^{-12}$	$25 \cdot 10^{-12}$
CEM I with fly ash	$4 \cdot 10^{-12}$	$15 \cdot 10^{-12}$
CEM III	$1 \cdot 10^{-12}$	$5 \cdot 10^{-12}$

Table 3.1. Chloride migration coefficient (m^2/s)

for the Portland cement, a is characterized by an average value of 0.3, and the characteristic time, t_0, is 28 day = 0.0767 years.

If, in Equation 3.10, x = represents the concrete cover, we obtain a function describing chloride concentration over time. When this concentration reaches the value C_{crit}, it indicates that the chlorides have reached a level sufficient to break down the protective oxide layer of the reinforcement and initiate corrosion. In MC 90, C_{crit} is considered 0.6 %, while Gjørv (2009) recommends a value of 0.4%. In general practice, a value of 0.5% is commonly used.

If the corrosion of the reinforcement occurs due to chloride attack, it will be localized. This type of corrosion is called pitting corrosion. However, if the corrosion begins due to the carbonation of the concrete, uniform corrosion will occur across all the bars.

3.1.3 Rebar corrosion

The mechanism involved is electrochemical and requires the presence of an electrolyte, typically an aqueous solution, that enables coupled anodic and cathodic reactions to occur. In reinforced concrete, this electrolyte is the interstitial pore solution, which allows ions to migrate from the anodic site to the cathodic site along the steel surface [21].

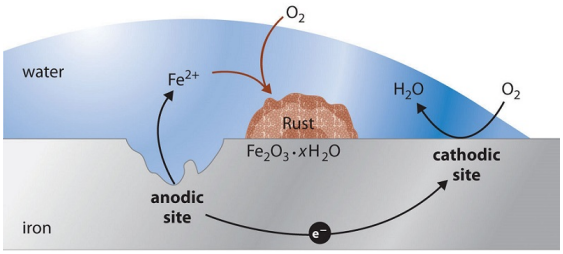

Figure 3.5. Scheme of steel corrosion process

During the process, the anodic 3.12 and cathodic 3.13 half-reactions occur simultaneously. The cathodic reaction is an oxygen reduction reaction that restores equilibrium by consuming the electrons released by the anodic oxidation reaction:

$$Fe \longrightarrow Fe^{2+} + 2e^{-} \tag{3.12}$$

$$2e^{-} + (\frac{1}{2})O_2 + H_2O \longrightarrow 2(OH)^{-} \tag{3.13}$$

In an electrochemical corrosion process, the conventional current flows from the cathode to the anode, while electrons move in the opposite direction, being supplied by the anodic sites. This electron release causes a reduction in the cross-section of the reinforcement bar at the anode, where material is progressively lost, whereas the cathodic regions experience increased protection due to locally higher alkalinity. However, the damage induced by reinforcement corrosion is not limited to local reductions in nominal steel area; it affects the entire bar. The anodic and cathodic products formed within the electrolyte react to produce iron hydroxide, which, in the presence of oxygen, can further transform into ferric hydroxide, a compound that precipitates as rust.

Rust occupies a much greater volume than the original steel, generating internal stresses within the concrete that can lead to the expulsion of the concrete cover (spalling). Once the cover is lost, the reinforcing bars become exposed and unprotected, creating conditions in which corrosion accelerates significantly.

Corrosion can be classified in several ways. The most common approach is based on its visible appearance, as some forms of corrosion can be readily identified, while others are not easily detectable. The most frequent types of corrosion affecting steel components are the following [31]:

- **Uniform corrosion**. Generating a uniform layer of rust (formation of oxide) over the surface of the metal exposed to atmosphere. In principle, uniform corrosion can reduce the rate of corrosion by limiting the contact surface between metal and the atmosphere.
- **Pitting Corrosion**.One of the most common forms of corrosion with local attack which sometimes taking the form of deep holes (pits) (figure 3.6) into steel surface. This kind of corrosion in the presence of imperfection in steel components or dirt on its surface can engender cracks;
- **Galvanic corrosion**. When two metals with different corrosive potential are placed together with the presence of a corrosive environment (electrolyte), the current flow and hence corrosion damage occur

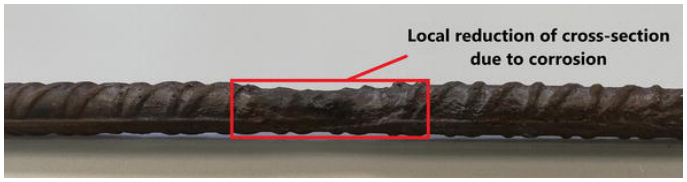

Figure 3.6. Pitting corrosion on a rebar [32]

- **Crevice Corrosion**.This type of localized corrosion occurs by the differences between ion concentration in dissimilar environments (different ion concentration) inside and outside of the small crevice.
- **Erosion Corrosion**.When flowing of fluid with the relatively high velocity attacks over the surface of the metal, it can remove the coating film and accelerate the corrosion process.
- **Stress Corrosion**.In the presence of corrosive environment and applied tensile stress brittle cracking occurs into the metal.
- **Fatigue Corrosion**.Repeated applied load with the corrosive environment causes stress concentration which leads to cracks into the metal.
- **Fitting Corrosion**.When two surfaces are in close contact in the presence of load provoke the abrasion of the surfaces by oxide.
- **Intergranular Corrosion** The corrosion attack between steel grain boundaries which affect the mechanical properties of the material.

This project considers only general corrosion and pitting corrosion. The former typically develops when the concrete cover becomes fully carbonated, while the latter is associated with chloride, induced attacks. Although both mechanisms are evaluated using the same computational approach, their effects are scaled according to the corresponding corrosion rate. It is also important to note that these forms of corrosion may occur simultaneously (Figure 3.7); for instance, an initial localized attack may develop first, followed by a more uniform corrosion process affecting the entire reinforcement.

The first step, to determine the rate at which reinforcement will lose diameter over time, is to calculate the corrosion rate i_{corr}, which is defined as the rate at which electrons move away from iron in anodic reactions ($\mu A/cm^2$). The corrosion rate will not remain constant during the propagation period, because many factors vary with time and with the characteristics of the structure, especially environmental

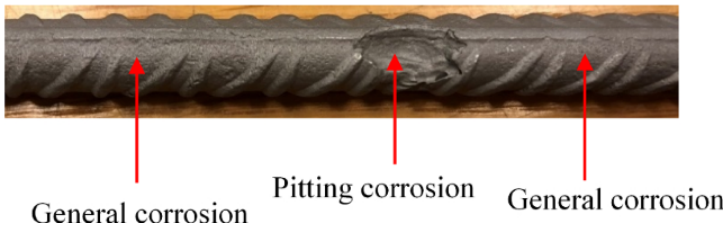

Figure 3.7. Different type of corrosion on a rebar [33]

factors. Fortunately, empirical models have been developed which, using a series of parameters and equations, allow corrosion rates to be calculated more simply [34]. Above, some models useful for this thesis project are reported.

The model 3.14 [Vu and Stewart (2000)] focuses on structures located in environments with a relative humidity of 75% and an average annual temperature of approximately $20°C$. This model takes into account the water-to-cement ratio (w/c) and, unlike the previous model, includes among its variables the concrete cover of the reinforcement.

$$i_{corr}(t) = 0.85 \cdot t_p^{-0.29} \cdot i_{corr_0} \tag{3.14}$$

where:
i_{corr} : corrosion rate ($\mu A/cm^2$);
$t_p = t_a - t_i$: is the propagation period (years). It is the active phase of corrosion, is computed as the age of the structure (t_a) minus the initiation time (t_i), in our case the time of carbonation or chloride attack ;
i_{corr_0} is the corrosion rate at the beginning of the corrosion propagation period ($\mu A/cm^2$).

$$i_{corr_0} = \frac{37.8 \cdot (1 - \frac{w}{c})^{-1.64}}{d_c}; \tag{3.15}$$

where:
w/c : water/cement ratio;
d_c : is the concrete cover depth (mm).;

It is a simple model suitable for practical applications. However, it is important to note that it does not account for environmental factors affecting the structure, such as relative humidity or ambient temperature.

The Model 3.16 [Li (2004)] develops a specific model for structures exposed to environments with high chloride concentrations, considering the following parameters: ambient temperature, relative humidity, w/c ratio, concrete cover, and chloride concentration on the position of the reinforcement.

$$i_{corr}(t) = 2.486 \cdot (\frac{RH}{45})^{1.6072} \cdot (\frac{T}{10})^{0.3879} \cdot (\frac{w/c}{0.35})^{0.4447} \cdot (\frac{d_c}{10})^{-0.2761} \cdot k_{cl}^{1.7376} \quad (3.16)$$

where:
i_{corr} : corrosion rate ($\mu A/cm^2$);
T : is the temperature in degrees kelvin at the position of the reinforcement ;
RH :is the relative humidity.
k_{cl} :is the chloride concentration on the position of the reinforcement (% weight of the concrete, and limited to 0.14–0.43%).

The Model 3.17 [Kong et al. (2006))] was carried out by a database (2927 results) obtained from seven-series specimens exposed to high chloride contamination over a time period of 5 years.

$$ln(i_{corr}(t)) = 8.617 + 0.618 \cdot lnC_t - \frac{3034}{T}) - 5 \cdot 10^{-3} \cdot \rho \quad (3.17)$$

where:
i_{corr} : corrosion rate ($\mu A/cm^2$);
C_t :is the chloride concentration at the reinforcement position (kg/m^3).
ρ : is the ohmic resistance of concrete ($ohms$).

$$\rho = \begin{cases} [27.5 \cdot (0.35 - \frac{w}{c}) + 11.1] \cdot (1.8 - C_t) + (1 - \frac{RH}{100})^2 + 40, & \text{if } C_t < 3.6\ kg/m^3 \\ 10, & \text{if } C_t > 3.6\ kg/m^3 \end{cases} \quad (3.18)$$

Once you have decided on the model to use to calculate the corrosion rate based on the information available, the characteristics of the concrete, and the environmental conditions, the diameter loss of the rebar is calculated using Equation 6.3.

$$P_x = 0.0116 \cdot i_{corr} \cdot t_p \cdot \alpha \quad (3.19)$$

where:
P_x : is the diameter loss (mm);
0.0116 :a conversion factor for steel from $\mu A/cm^2$ to $(mm/year)$.
α : is the a pitting factor normally adopted for corrosion caused by chloride attack, it could be set in a range between 4 and 8 [35].

With the information described in this section, it is now possible to calculate the loss of reinforcement cross-section over time. The next step is to determine when the swelling of the reinforcement due to corrosion leads to concrete splitting and spalling.

3.1.4 Splitting and Spalling

The phenomenon of splitting and spalling is of fundamental importance for reinforcement in the compressed zone. Splitting causes a decrease in the compressive strength of concrete, while spalling leads to a reduction in the resistant section. The swelling of reinforcing bars caused by corrosion leads to deformation of the concrete section [23]. The transverse deformation of the section's bulging can be expressed as:

$$\epsilon = \frac{b_f - b_i}{b_i} \tag{3.20}$$

where:
b_f : the section base after the deformation;
b_i : the initial section base;

The increase in the base dimension can be expressed as a function of the average crack opening due to corrosion-induced splitting, as follows:

$$b_f - b_i = n_{bar} \cdot w(t) \tag{3.21}$$

$w(t)$ indicates the average crack opening for each reinforcement bar.
From Equations 3.32 and 3.21:

$$\epsilon = \frac{n_{bar} \cdot w(t)}{b_i} \tag{3.22}$$

The average crack opening for each bar can be estimated as:

$$w(t) = \begin{cases} 0, & \text{x} < x_0 \\ w_0 + \beta \cdot (x(t) - x_0), & \text{if } C_t{>}3.6kg/m^3 \end{cases} \tag{3.23}$$

$w_0 = 0.05mm$: represents the opening of an intrinsic crack from initial splitting; β : constant parameter that can be assumed to be 0.009 $mm/\mu m$; $x(t)$: is the depth of corrosion, evaluated as described in the previous paragraph,; x_0 : represents the depth of corrosion necessary to produce the first splitting crack.

$$x_0 = a_1 + a_2 \cdot \frac{c}{\phi} + a_3 \cdot f_{c,sp} \tag{3.24}$$

where:
$a_1 = 74.4\ \mu m$; $a_1 = 7.3\ \mu m$; $a_1 = -17.4\ \mu m$;
c : cover concrete depth mm;
ϕ : is the largest diameter in the considered group mm;
$f_{c,sp}$: is the characteristic resistance to splitting traction.

$$f_{c,sp} = \frac{f_{ct,0.95}}{0.9} \tag{3.25}$$

Compressive strength decreases due to the presence of tensile forces and transverse cracks. The estimation can be performed using Equation 3.28:

$$f^* = \frac{f_c}{1 + 0.001 \cdot \frac{\epsilon_t}{\epsilon_{co}}} \tag{3.26}$$

ϵ_{co} is the deformation due to the peak of compression stress and could be estimated as:

$$\epsilon_{co} = 0.0017 + 0.0010 \cdot \frac{f_{cm}}{70} \tag{3.27}$$

When the opening of the splitting cracks reaches $w(t) = 1\ mm$,it is reasonable to assume that the concrete cover can no longer withstand the tensile stresses and will eventually detach. Since the tensile concrete portion is not considered in the structural design, its loss does not represent a significant reduction in the load-bearing capacity of the member. However, the detachment of the cover has a major impact on the corrosion process: once the reinforcement is exposed, it is no longer protected by the alkaline environment of the concrete, and the corrosion rate increases significantly.

3.1.5 Protection and Maintenance

The objectives of maintenance and protection are to prevent or slow down degradation processes in both concrete and reinforcing steel through preventive measures; to restore the mechanical and functional performance of the structure through corrective interventions; and, more broadly, to extend the service life of the structure while ensuring adequate levels of safety and functionality. Equally important is the consideration of costs, which can be optimised by adopting planned maintenance strategies rather than relying on delayed, extraordinary interventions.

Carbonation

To prevent this type of deterioration in reinforced concrete, as shown by the models presented in Chapter 3.1.1, it is highly beneficial to optimise the concrete mix design. Beginning with the water-to-cement ratio, which must be selected based on strength and workability requirements, it is advisable to also consider the carbonation rate as a design parameter, since an increase in the water-to-cement ratio leads to a corresponding increase in carbonation depth.

The models also highlight the fundamental role of aggregate selection. Aggregates with high water absorption accelerate the diffusion of CO_2 through the cement paste. Finally, proper curing is essential: preventing early-age cracking and ensuring adequate concrete strength significantly slows the carbonation process. Taken together, these measures represent a crucial and cost-effective first step toward maintaining the durability of the structure.

In addition to optimising the concrete mix design, further protective techniques can be employed. Organic coatings and penetrating sealers, for example, can be applied to create barriers that either obstruct micropore pathways or render the surface hydrophobic, thereby reducing CO_2 ingress. Reviews indicate that such coatings can significantly delay carbonation on exposed surfaces, although their effectiveness depends on factors such as coating type, penetration depth, and maintenance requirements [36].

For the purposes of this study, it is essential to account for the deterioration of these protective systems. As these materials age, their resistance to carbonation gradually decreases. This decline in performance is attributed to ageing-related defects in organic coatings, including granulation, increased porosity, and cracking. Under natural ageing conditions, the service life of these coatings has been reported to range between 1.5 and 3.0 years [37].

To estimate the cost of applying such coatings, the regional price list for the

Piedmont region was consulted. However, since no specific item corresponding to these coating types was available, the following item was considered:

> Deep impregnating treatment for anti-degradation protection and waterproofing, consisting of sodium silicate (liquid glass) in a ready-to-use aqueous solution, colourless, odourless, and non-toxic. This treatment is designed to improve the chemical, physical, and mechanical characteristics of concrete, such as hardness, compactness, and impermeability, and is to be applied to new or renovated surfaces in two coats, excluding any surface cleaning and preparation.

The price list states that for concrete structures with a surface area of over 400 m^2 applied using a low-pressure electric spray pump, the cost is 9.49 €/m^2 [38].

Of course, determining an appropriate concrete cover is essential for ensuring structural durability, as reinforcement corrosion begins once carbonation reaches the full depth of the cover. At the same time, the influence of the cover thickness on the overall weight of the structure, as well as on its aesthetic characteristics, must also be taken into account. As discussed in this section, protecting the structure from carbonation requires a combination of several interacting factors, each of which affects other structural properties. For this reason, an optimised mix design is crucial, allowing all relevant performance requirements to be balanced effectively.

Chloride attack

As can be seen from Section 3.1.2, investigations with various types of cement confirmed that the diffusion of chloride ions is strongly influenced by cement composition. For example, blended cement pastes containing pulverized fuel ash or granulated blast furnace slag showed lower diffusion rates at 25°C than ordinary Portland cement pastes with the same $\frac{w}{c}$ ratio, and these differences could not be explained solely by variations in the pore structure of these materials. The $\frac{w}{c}$ ratio also has a strong influence on the diffusion coefficients (Figure 3.8), as the pore structure depends on it.

As with carbonation, chloride attack can also be slowed down by using coatings. In particular, studies have shown that this protection can delay chloride penetration to the rebars depending on the type of coating, with an average effectiveness of 3.5 years [40]. The cost is considered similar to that of coatings for carbonation.

Designing an appropriate concrete cover is essential for extending the service life of the structure, as it increases the distance chloride ions must travel to reach the reinforcement and initiate corrosion.

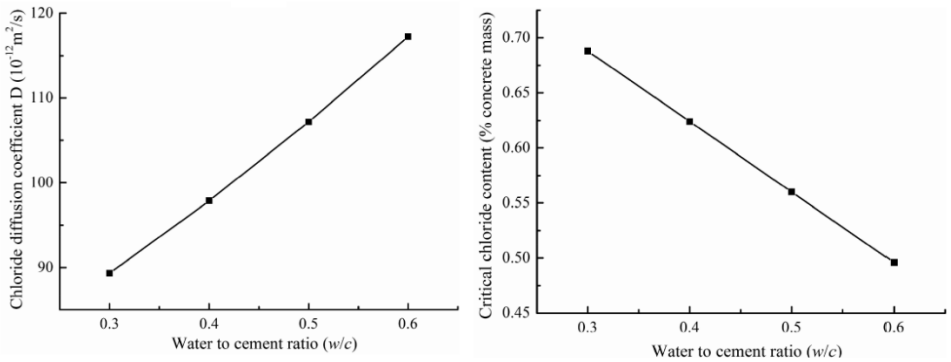

Figure 3.8. Influence of the w/c ratio on the critical chloride content and diffusion coefficient [39]

Rebars corrosion

In studies on corrosion mitigation in reinforced concrete, the quantitative reduction in corrosion rate varies considerably depending on the protection strategy adopted, the exposure conditions, and the condition of the protective layer.

In the first part of this analysis, the methods used to reduce the corrosion rate are examined. As discussed in Section 3.1.3, an appropriate mix design is fundamental for limiting corrosion; however, when this alone is insufficient, several additional protection strategies can be adopted. One of the most widely used systems in reinforced concrete structures combines epoxy-coated reinforcement with an increased concrete cover. This approach has demonstrated significant improvements in corrosion performance compared with uncoated bars [41].

This study considers several reinforcement protection techniques that mitigate corrosion through different mechanisms. For analytical purposes, an average corrosion-rate reduction factor of approximately 4 has been assumed, meaning that protected reinforcement is expected to corrode roughly four times more slowly than unprotected steel. In this case, the Piedmont region's price list provides a clear description of the application procedure for this method and its associated cost:

> Application of a corrosion inhibitor, applied with a brush or spray, to prevent further oxidation of steel reinforcement and ensure the anchoring of cement mortar coatings. This includes brushing of the reinforcement; the cost is 9.56 €per linear metre of treated steel.

This application can be carried out during the construction phase of the structure to prevent corrosion, and similarly, it can be applied during the maintenance

phase. When the reinforcement is already corroded, maintenance on the concrete structure should proceed as follows: the deteriorated concrete is removed to expose a sound substrate and the corroded reinforcement [42]. Concrete removal can be performed by mechanical means or hydrodemolition, taking care not to damage the reinforcement [43].

Subsequently, the steel reinforcement is cleaned to remove corrosion products and rust scales. After cleaning, it is treated with a passivating or protective coating. These coatings, often cementitious or polymer-modified, help reestablish the alkaline environment and prevent further corrosion. Where section loss exceeds allowable limits, the reinforcement should be repaired or supplemented with new bars to restore the cross-sectional capacity [44].

The next stage involves recasting or patching the removed concrete using compatible repair mortars or concrete. In some cases, a bonding slurry or agent is applied before placing the repair mortar. Proper curing is essential to prevent shrinkage cracking and to achieve full strength development [45]. Once the repair mortar has hardened, it is possible to carry out the surface treatment described in the previous paragraph to slow down carbonation and chloride attack.

The Piedmont region's price list dedicates an item to this type of maintenance.

> Repair and restoration of missing parts of concrete carried out with premixed fibre-reinforced mortar, class R3, synthetic resins and aggregates of suitable size, for a total thickness of up to 30 mm, excluding formwork and any reinforcing bars for implementation, including the removal of damaged parts until the sound conglomerate is reached, cleaning by manual brushing or other suitable means, including treatment of existing bars with converting or passivating products. The cost is measured per damaged area, 197.61 €/m^2

After maintenance, the product regains its original characteristics, allowing the prediction–maintenance cycle of deterioration to be considered as restarting from the beginning.

For the sake of completeness, although they are not included in the analyses of this study, it is worth introducing fibre-reinforced polymers (FRP), which have gained significant recognition in recent years in civil engineering as materials for enhancing the structural integrity of reinforced concrete (RC) structures. FRP systems are highly effective in increasing the load-carrying capacity and stiffness of RC beams, which has driven widespread interest in flexural strengthening techniques. These reinforcements are typically produced through the pultrusion process and

incorporate various types of fibres, including carbon (CFRP), glass (GFRP), basalt (BFRP), and aramid (AFRP).

E-GFRP is the most commonly used due to its relatively low cost, whereas BFRP, although more expensive, offers higher strength, excellent alkali resistance, and an abundant raw-material supply. AFRP, characterised by low compressive strength and high cost, is not widely used for structural bars but is suitable for applications such as ballistic-resistant textiles. CFRP provides the highest strength and the broadest range of mechanical properties among FRP materials, owing to the nature of the carbon fibres and the production process. It also exhibits superior resistance to fatigue and creep compared with other FRP types. Despite its higher cost, CFRP's exceptional strength and durability under cyclic loading make it a preferred choice for demanding applications. Table 3.2 summarises the key mechanical properties of FRP composites [46].

Code	Tensile strength (MPa)	Modulus of elasticity (GPa)	Ultimate strain
CFRP	1200–2250	100–147	0.012–0.017
GFRP	600–710	30–46.4	0.015–0.020
AFRP	70–123	2.3–3.4	0.014–0.043
BFRP	1000–1100	50–70	0.022

Table 3.2. FRP properties [47]

However, when using FRPs, several aspects must be taken into account, including the increase in structural rigidity and crack resistance. At the same time, it is essential to consider the corresponding reduction in deformability and ductility. In this project, these effects were not analysed, both due to the complexity associated with modelling their influence and the limited availability of reliable information on the long-term degradation of these materials.

3.2 Carbon steel

The general discussion regarding steel corrosion has already been presented in Section 3.1.3. To study the progression of corrosion depth over time in carbon steel, the paper [48] was analyzed in order to estimate the corrosion depth during the first year. This study examines three major international programmes on atmospheric corrosion: ISOCORRAG, ICP/UNECE and MICAT. Although each programme has its own specific characteristics, the similarity of their basic methodologies allows the corresponding databases to be combined and compared.

The paper examines the influence of climatic parameters, such as humidity, temperature, rainfall, and pollutant concentration, on the annual corrosion rates of carbon steel. This work forms part of a broader international effort involving global exposure programmes aimed at understanding how environmental factors govern material degradation. The authors analysed long-term datasets, comparing corrosion behaviour across different continents and climatic zones. The study correlated the measured corrosion rates with key environmental indicators, including time of wetness (TOW), chloride deposition, and sulfur dioxide concentration, all of which are known to influence electrochemical processes on metal surfaces.

Over the years, numerous predictive models have been proposed to estimate the atmospheric corrosion behaviour of carbon steel. The scientific literature includes a wide range of damage functions that relate corrosion rates to environmental and climatic parameters. However, the applicability of many of these models is limited, as they were often developed under narrowly defined climatic conditions or within restricted geographical regions, resulting in only minimal variability in the key meteorological parameters.

Notable contributions include the pioneering work of [49], who sought to formulate universal corrosion equations incorporating atmospheric pollutant concentrations, meteorological factors, and rainfall acidity (pH). Their study also involved an extensive review and statistical analysis of global datasets on atmospheric corrosion and environmental conditions, from which they derived generalised corrosion functions expressed through simple climatic and pollution-related parameters.

In recent decades, the databases established through the ISOCORRAG, ICP/UNECE, and MICAT programmes have enabled the development of stronger correlations between atmospheric corrosion rates, pollution levels, and climatic variables. The consolidation of data from these initiatives provides a robust foundation for formulating damage functions that are globally applicable and representative of a wide range of environmental conditions. This integration forms the core objective of the present study, in which the available data have been analysed using a linear regression model to quantify the dependence of corrosion rates on key environmental parameters.

The Authors [48] fitted the data in relation of the following linear equation:

$$C = a_1 + a_2 \cdot RH + a_3 \cdot P + a_4 \cdot T + a_5 \cdot TOW + a_6 \cdot SO_2 + a_7 \cdot Cl \qquad (3.28)$$

where:

C : Carbon steel annual corrosion (μm);
RH :annual average relative humidity (%).
T : annual average temperature ($^{\circ}C$).
P : annual precipitation (mm).
TOW : time of wetness, annual fraction of number of $hours/year$ in which $RH >$ 80% and $T > 0\ ^{\circ}C$.
$SO2$: $SO2$ pollution in mg/m^2 in a day.
Cl : Cl pollution in mg/m^2 in a day.

The coefficients $a_2 - a_7$ represent the relative weight of each variable in the equation, while $a_1$acts as the constant term. The authors employed a least-squares regression model, in which the coefficients $a_1 - a_7$, are determined by minimising the squared differences between the observed values and those predicted by the model.

The authors derived several equations based on the different databases considered. However, according to their conclusions, the following equations proved to be the most reliable. To evaluate the quality of the model fit with respect to the experimental data, the coefficient of determination R^2 was used. This statistic, equal to the square of the multiple correlation coefficient, expresses the proportion of the variance in the dependent variable that is explained by the independent variables.
In non-marine environment:

$$C = -26.32 + 0.45 \cdot RH + 0.43 \cdot T + 0.82 \cdot SO_2 \tag{3.29}$$

In relation to marine envirnoment, the damage function obtained is:

$$C = -24.50 + 0.75 \cdot Cl + 0.67 \cdot SO_2 + 77.32 \cdot TOW \tag{3.30}$$

If the objective is to analyse short-term corrosion rates, these models provide an excellent fit. However, in most practical applications, it is necessary to evaluate long-term corrosion behaviour.

Although numerous long-term models have been proposed in the literature, the most comprehensive is the one developed by [50]. This model is based on the well-known power law introduced earlier in Section 3.1.3, which predicts corrosion loss as a function of time alone. To extend this time-dependent formulation by incorporating several environmental adjustment factors, the following model was proposed to estimate corrosion loss:

$$y = A \cdot t^B (\frac{TOW}{C})^D \cdot (1 + \frac{S0_2}{E})^F \cdot (1 + \frac{Cl}{G})^H \cdot e^{J \cdot (T + T_0)} \tag{3.31}$$

where:
y : Corrosion Loss (μm);
t : exposure time ($years$);
TOW : time of wetness, annual fraction of number of $hours/year$ in which $RH >$ 80% and $T > 0$ $^\circ C$;
$SO2$: $SO2$ avarage concentration mg/m^3;
Cl : Cl deposition rate $mg/m^2/day$;
T : air temperature ($^\circ C$);
$A, B, C, D, E, F, G, H, J$: Empirical coefficients;

The ISO CORRAG dataset, obtained from 51 test sites across 13 countries, was used to calibrate the coefficients of the eight models. Considerable attention was given to the selection of these locations, ensuring a broad range of environmental conditions so that the influence of climatic and pollution-related factors on corrosion could be accurately represented.

The effect of environmental exposure was investigated for four metals: carbon steel, zinc, copper, and aluminium. For each material, two specimen types were tested: flat panels measuring $100 \times 150 \times 2$ $mm$and helical wires with a diameter between 2 – 3 mm and a length of 1 m. Based on this comprehensive dataset, the empirical coefficients were derived and are reported in Table 3.2. Following preliminary assessment, the reference values used in the model were set as follows:

- $T_0 = 20$ $^\circ C$;
- $C = 3800$ $hours/year$
- $E = 25$ $\mu g/m^3$
- $G = 50$ mg/m^2

3.2.1 Protection and Maintenance

Considering that steel structures are almost always galvanised, the load-bearing section does not immediately lose material. The protective zinc coating, available in different forms (Figure 3.9), must first be completely consumed before corrosion of the steel begins. Zinc provides sacrificial protection, consistent with the corrosion mechanisms described in Section 3.1.3, by acting as the anodic material in the galvanic system.

Materials	Type	A	B	D	F	H	J
Carbon Steel	Flat	13.4	0.98	0.46	0.62	0.34	0.016
Carbon Steel	Helix	19.7	0.05	0.46	0.62	0.34	0.016

Table 3.3. Empirical Coefficients about Carbon Steel of the long-term corrosion model

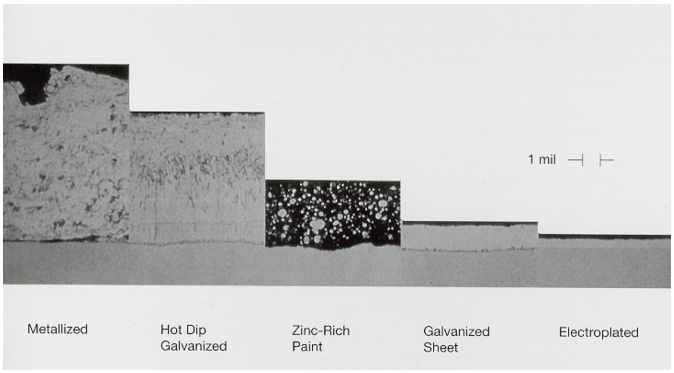

Figure 3.9. Different zinc coating protection [51]

Through this process, zinc corrodes preferentially, shielding the underlying steel from moisture and oxygen. As long as the zinc layer remains, it forms stable corrosion products that continue to protect the substrate. Once the coating is depleted, however, the steel becomes exposed and corrosion of the structural section can begin.

When exposed to the atmosphere, the zinc coating undergoes a natural weathering process that leads to the formation of a protective layer of zinc carbonate. This patina can, however, deteriorate under certain environmental conditions [6], such as:

- High humidity. In tropical climates or areas with persistent moisture, zinc corrosion tends to accelerate.
- Coastal and marine environments. Elevated sodium chloride levels can intensify the erosion of the zinc coating.
- Polluted atmospheres. Industrial regions with sulphur dioxide emissions or urban areas affected by vehicle exhaust can cause deterioration of the zinc's protective layer.

To estimate the annual corrosion rate under specific environmental factors, such as temperature, humidity, salinity, and pollutant concentration, the Zinc Coating Life Predictor could be used. It is a power tool developed by the American Galvanizers Association [51].

In addition, building on the model already discussed in this section, the study [50] also provides empirical coefficients for zinc, as reported in Table 3.2.1. Consequently, when the presence of a zinc protective layer is considered, corrosion of the underlying carbon steel will only initiate once the time required to consume the entire thickness of the zinc coating has elapsed.

Materials	Type	A	B	D	F	H	J
Zinc	Flat	0.16	0.36	0.24	0.82	0.44	0.05
Zinc	Helix	0.26	0.05	0.24	0.82	0.44	0.05

Table 3.4. Empirical Coefficients about Zinc of the long-term corrosion model

When the steel structure is new, the structural elements arrive already galvanised, which can be done in two ways:

- Electrolytic galvanising;
- Hot-dip galvanising.

The galvanising process takes place by immersion, meaning the metals are immersed in working baths to achieve the treatment. Electrolytic galvanising is a galvanic deposition process that produces a thin zinc coating on the metal surface (5–12 μm), offering good aesthetic qualities and paintability. It is a delicate process involving several treatment stages. Hot-dip galvanising involves immersing the elements in a bath of molten zinc, producing a much thicker zinc layer (15–75 μm), but with poorer aesthetic qualities and more difficult paintability.

Full Repainting

When the galvanised coating has been completely consumed, long-lasting protective systems represent the most effective solution, particularly when considering factors such as product life cycle, manufacturing cost, and maintenance requirements. In this study, two options were selected: thermal-spray zinc coating, which involves spraying molten zinc onto a previously sandblasted steel surface [52], and inorganic zinc-rich coatings, durable paint-like systems that provide excellent corrosion protection through metallic zinc dust dispersed in a silicate binder.

In [53], the corrosion resistance of the coatings was analyzed. Based on the results predicted by the model, if an accelerated salt-spray treatment is adopted and the coating is highly reliable, it takes about 40 years for the thermal-spray zinc coating to be reduced by 200 μm, while it takes about 40 years for the inorganic zinc coating to be reduced by 75 μm. The thickness of the conventional thermal-spray zinc coating is about 250 μm, and that of the inorganic zinc-rich coating is about 100 μm. Therefore, we can safely conclude that both types of coatings, if applied correctly, will last for at least 40 years.

The costs for applying these protective coatings could not be found in the Piedmont region price list. However, the following prices were found for the application of the protective spray alone: 60–70 €/ m^2. Considering that the metal surface must be cleaned before applying the coating, the cost of sandblasting should be added, which, according to the Piedmont region price list, is 19.56 €/ m^2. Therefore, the total maximum cost for the application can be considered as 89.56 €/ m^2.

In conclusion, there are various methods of steel maintenance. For example, if localized corrosion is detected, it can be repaired by local repainting or through techniques such as Impressed Current Cathodic Protection (ICCP). A cathodic protection system essentially controls the steel potential using a continuous current source, making the steel potential more negative and thereby suppressing corrosion [54]. However, these methods are not considered in this study because corrosion is assumed to be uniform across the structure. Global repainting is considered instead. While ICCP effectively prevents corrosion, its operation is very expensive, particularly in terms of sensor maintenance, and for a bridge of the size considered here, it would be an unreasonable cost.

Repair section

In the transportation sector, several techniques are used to address section loss in metal bridge structures. Before planning any intervention, it is essential to identify the cause of the deterioration. The client should therefore consider whether the origin of the problem can be eliminated or mitigated, as this affects the choice of repair technique and design criteria.

The most common solutions consist of plating (Figure 3.10), partial replacement of the element, or complete replacement of the damaged section.In most cases, section loss is resolved by applying additional plates to the existing element. In fact, “plating” indicates the addition of sheets or other metal elements which, connected to the original member, form a composite section. This method is used both to increase strength and to improve load-bearing capacity; in many cases it

can also lead to improved element evaluation.

When degradation is very pronounced, or when the geometry of the damaged area makes plating impractical, partial or total replacement of the structural element is resorted to. This solution is particularly effective near the connections or supports, where numerous layers of additional sheet metal would be needed to restore the required capacity. Among the areas most subject to such interventions are the nodal plates (gusset plates) and the ends of the beams, especially in correspondence with supports or joints with other transverse and longitudinal elements.

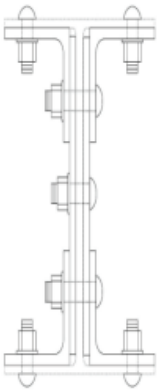

Figure 3.10. Plating an existing W-shape with angles and flat plate

Studies are also underway on alternative technologies to plating or replacing damaged elements. Solutions currently under research include synthetic coatings such as fiber-reinforced materials, ultra-high-performance concrete stacking, and thermal application of metals to reconstruct the original cross-section [55].

In general, the materials used are carbon-fibre-reinforced polymers (CFRP). The mechanical properties of the CFRP composite depend on many factors, including the percentage of carbon fiber and the type of matrix used. Consequently, mechanical properties vary from one CFRP manufacturer to another. However, mechanical properties such as Young's modulus and tensile strength are several times higher than those of conventional steel. With CFRP composites, as with other polymers, the glass transition temperature is very important. The glass transition temperature is the temperature at which the transition from the liquid state to the plastic or glassy state occurs. This is manifested by a step increase in the viscosity of the substance. The glass transition temperature for CFRP composites mainly depends on the type of polymer matrix used. As already mentioned, the use of these fibres is certainly easier than reconstructing the section with plating;

however, their effectiveness depends on many factors, such as the direction of fibre application, and their use can also lead to a reduction in the ductility of the structure.

3.3 Cables

A cable may be composed of one or more structural ropes or structural strands. A strand (with the exception of parallel wire strands) is an assembly of wires formed helically around a center wire in one or more symmetrical layers. A rope is composed of a plurality of strands helically laid round a core [56]. Considering that metal corrosion in science is always described by the expression [57]:

$$C(t) = A \cdot t^n \tag{3.32}$$

Starting from this expression, a simplification was made. Specifically, it was assumed that the steel of the cables corrodes according to the same Model 3.31described in Section 3.2, even though the two elements are made of different types of steel. This choice was motivated by the fact that, despite the differences in composition, they undergo the same chemical corrosion mechanisms. Moreover, this model was adopted because no corrosion model as general and widely applicable as the one analysed in that section was found. Existing corrosion models for cables do appear in academic literature, but they are all based on very specific environmental assumptions and therefore are not suitable for the broader conditions considered in this study.

Unlike steel profiles, the cables of suspension bridges are not only protected by galvanisation but also benefit from additional protection from the external environment, as they represent the most critical structural element.

3.3.1 Protection

The conventional corrosion-resistant system for typical suspension bridge cables is shown in Figure 3.12. A cable is composed of high-strength steel wires, each of which is galvanised with a zinc coating approximately μm thick. . After galvanisation, each wire is further protected with a primary coating to prevent damage during construction. Once all the wires are installed on site, they are compacted into a circular shape, and the exterior surface is covered with an anti-corrosion paste. The compacted cable is then wrapped with annealed galvanised steel wires, and the outer wrapping is finally protected by a paint-applied coating system.

This system has remained largely unchanged since its first use on the Brooklyn

Figure 3.11. Corrosion on the side of a cable from the Innoshina Bridge [58]

Bridge more than 100 years ago. Steel wires are typically galvanised, although exceptions exist. One such case is the Williamsburg Bridge, whose ungalvanised wires exhibited significantly poorer corrosion performance compared with galvanised wires. For this reason, galvanisation of steel wires is strongly recommended to reduce corrosion risk.

Red lead has been used almost exclusively as the paste material in the United States and Europe. Japanese suspension bridges, by contrast, have employed a mixed paste consisting of calcium plumbate, high-molecular organic lead, calcium carbonate, and linseed oil. Although such pastes have traditionally been used to enhance corrosion resistance in conventional suspension bridges, they are no longer applied when dehumidification systems are installed, as dry air circulating through the spaces between the outer and wrapping wires provides more efficient protection [59].

In [60], a comprehensive field investigation was conducted to assess cable corrosion on several Japanese suspension bridges. When the protective wrapping wires were removed, water was consistently found in the lower sections of the main cables across all inspected bridges. In some cases, a substantial amount of water drained from the cables immediately after unwrapping. A dark brown discoloration caused by steel rust was visible on the light brown surface of the anticorrosion paste, particularly along the sides and lower portions of the cables. After the paste was removed, partial depletion of the zinc coating and visible steel corrosion were observed. The side regions exhibited the most severe deterioration, with the lower portions also significantly affected. Several outer layers of galvanised wires showed extensive corrosion and red rust formation.

Two primary factors were identified as potential causes of water ingress within

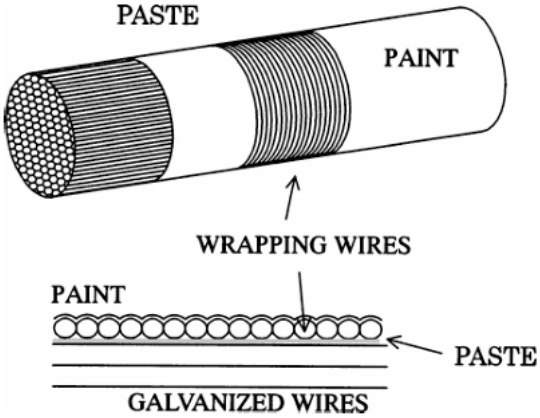

Figure 3.12. Corrosion resistant system of Suspension bridge cables

the cables. First, during cable erection, which may span several years, rainwater can enter through gaps between wires and become trapped. Second, even after the cables are completed and sealed with wrapping wires and paint, water may infiltrate through damaged sealants at cable bands or through cracks in the paint layer.

The internal environment of the cables was monitored in terms of relative humidity and temperature over a 24-hour period. Relative humidity remained nearly 100% throughout the cables, except in the upper region, where it dropped to about 85% in the afternoon. The upper portion maintained higher temperatures than the surrounding air, while the side sections were cooler in the morning and warmer in the late afternoon. Temperatures at the center and lower parts remained almost constant and were largely unaffected by external variations.

Based on these observations, the internal microclimate of the cable can be characterised as follows: at the top, nighttime cooling leads to dew formation on the wire surfaces, which partially evaporates during the day, leaving the wires wet at night and relatively dry during daylight hours. Along the sides, dew also forms overnight, but daytime heating is insufficient to fully dry the wires, resulting in persistently damp conditions. In the central region, limited temperature fluctuation prevents condensation, although humidity remains high. The lower portion of the cable remains continuously saturated with water.

From this information, it can be concluded that wrapping and corrosion paste have negligible influence on corrosion processes driven by temperature and relative humidity. However, they do provide effective protection against pollutants

such as Cl and SO_2, which significantly accelerate corrosion. Therefore, an accurate analysis must account for the internal environmental conditions of the main cable. Corrosion can thus be studied in a manner similar to that of carbon steel, considering the presence of a zinc coating and the fact that the wires are exposed to an environment with distinct influencing factors.

3.3.2 Maintenance

Cable maintenance represents a highly specialised area within bridge engineering. As discussed earlier, cable protection systems consist of multiple layers and components, each fulfilling a specific function in preventing corrosion and ensuring long-term durability. Consequently, the associated maintenance costs are closely linked to the overall bridge configuration and to the particular protective system employed.

For cost-estimation purposes, it is reasonable to refer to the values presented in Section 3.2, which outline the expenses associated with applying a new coating. However, maintenance operations involve additional tasks that must not be overlooked, most notably the labour required to remove and subsequently reinstall the outer protective layers, such as wrapping wires and anticorrosion paste. As a result, the overall maintenance cost per m^2 can be considered approximately three times higher than that of standard carbon-steel maintenance. This figure should nevertheless be regarded as indicative rather than exact, as material prices, site accessibility, and the specific installation techniques adopted can vary significantly between bridge projects.

In conclusion, for this type of intervention, pricing is more likely to be expressed per linear metre rather than per square metre, since the surface area requiring maintenance on tendons and cables is relatively small. Adjusting the pricing method in this way is therefore necessary to ensure the economic viability of the work.

Chapter 4

Ageing of a suspended bridge: general design and environmental conditions

The following chapter presents the analysis of a small suspension bridge. The objective is to develop a procedure through which the models described in the previous chapters can be applied to design and manage the structure in the most effective manner. For this purpose, the bridge deck was designed in two alternative configurations: one using steel and the other using reinforced concrete.

The case study was created specifically for this project. The suspension bridge (Figure 4.1) has a span of 40 m, with tendons positioned every 10 m, resulting in a total of three tendons. The carriageway was assumed to be 7 m wide, comprising two traffic lanes of 3 m each. The bridge was analysed in the two aforementioned configurations, steel deck and concrete deck. For the main cables, a section composed of multiple strands was adopted, with each strand consisting of seven wires.

The pylons supporting the main cable were assumed to be 7 m high, and the main cable in its unloaded configuration was modelled as a parabolic curve [61]. In addition, the cable was taken to be 1 m above the deck at mid-span. These assumptions made it possible to derive the function presented in Equation 4.1, which describes the cable profile and allows the calculation of both the total cable length and the individual hanger lengths.

$$y = \frac{3}{200}x^2 - \frac{3}{5}x + 7 \tag{4.1}$$

Initially, a preliminary design was carried out to verify the correct dimensioning of the structural elements. The Italian building code NTC 2018 was used as the

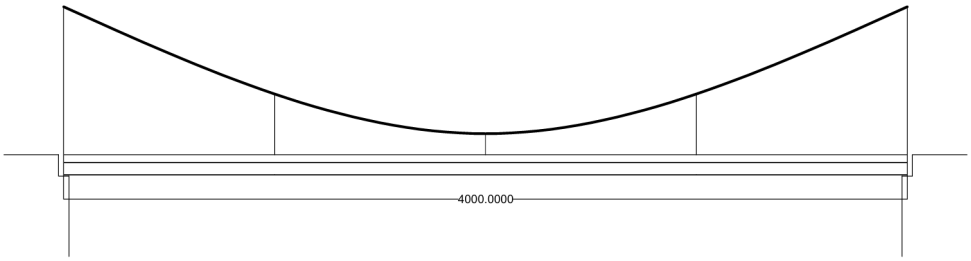

Figure 4.1. Suspended bridge case study

reference standard for the bridge design. Since the main objective of this thesis is not the structural design itself, only the verification of the ultimate limit state (ULS) was performed. In particular, the adopted load combinations include the safety coefficients shown in Figure 4.2.

In determining the loads acting on the bridge, only permanent actions and variable traffic loads were considered. Because two different deck types were analysed, the permanent structural loads differ between the two configurations, whereas the permanent non-structural loads and the variable traffic loads were assumed to be identical.

		Coefficiente	EQU[1]	A1	A2
Azioni permanenti g_1 e g_3	favorevoli sfavorevoli	γ_{G1} e γ_{G3}	0,90 1,10	1,00 1,35	1,00 1,00
Azioni permanenti non strutturali [2] g_2	favorevoli sfavorevoli	γ_{G2}	0,00 1,50	0,00 1,50	0,00 1,30
Azioni variabili da traffico	favorevoli sfavorevoli	γ_{Q}	0,00 1,35	0,00 1,35	0,00 1,15
Azioni variabili	favorevoli sfavorevoli	γ_{Qi}	0,00 1,50	0,00 1,50	0,00 1,30
Distorsioni e presollecitazioni di progetto	favorevoli sfavorevoli	$\gamma_{\varepsilon 1}$	0,90 1,00[3]	1,00 1,00[4]	1,00 1,00
Ritiro e viscosità, Cedimenti vincolari	favorevoli sfavorevoli	$\gamma_{\varepsilon 2}$, $\gamma_{\varepsilon 3}$, $\gamma_{\varepsilon 4}$	0,00 1,20	0,00 1,20	0,00 1,00

Figure 4.2. Partial safety coefficients for load combinations at ULS [62]

To dimension the structural section, the rule of thumb based on dividing the

span by 25 was adopted. In this case, the reference span corresponds to that of the hangers; however, since hangers do not behave as conventional supports, the preliminary section was increased accordingly. Specifically, an IPE 550 profile was selected for the steel deck, while a total depth of 700 mm was adopted for the reinforced-concrete section.

For both bridge configurations, the deck was assumed to be completed using Predalles-type prefabricated elements. The beams were spaced 5 m apart, and for this spacing, a prefabricated slab element with a height of 20 cm was adopted. The road surfacing system consists of a 5 cm screed placed directly above the Predalles elements, topped by a 3 cm asphalt layer. In addition to these loads, the side protection barriers were also taken into account, with a weight of 8.5 kg per 2 metres. For the calculation of variable actions, the equivalent distributed load of a 44 *ton* vehicle was considered, corresponding to 9.5 kN/m^2.

To pre-design the tendons, it was assumed that each tendon carries the entire load acting on its corresponding 10-metre span. Accordingly, for each tendon, the previously defined weights, already multiplied by the appropriate partial safety coefficients, were considered over a 10 m length of bridge. This load was then assumed to be fully transferred to the tendon, enabling the required steel area to be calculated as the ratio between the applied force and the strand resistance. Once the necessary area was obtained, and knowing the cross-sectional area of a single strand, the number of strands required for each tendon could be determined.

Finally, to pre-dimension the main cable, the solution proposed by [61] was considered, which takes the value $\frac{q_{tot} \cdot L^2}{8 \cdot f_0}$ as the horizontal force acting on the cable, where f_0 is the vertical distance between the pylons and the lowest point of the cable, and $\frac{q_{tot} \cdot L}{2}$ as the vertical force. This makes it possible to calculate the normal force acting at each point of the cable and subsequently dimension it. To perform this, the most critical loading condition was considered. The required number of strands was then calculated in the same manner as for the tendons. With all this information, the total weight acting on the bridge could be determined.

With all the information described above, it was necessary to determine an appropriate modelling strategy for the structural analysis. The main challenge was to develop a model that could be re-analysed repeatedly with low computational cost, since the simulation had to be performed year by year while progressively reducing the effective cross-section of the structural elements.

It was therefore assumed that the main cable would retain its original geometry

throughout the entire service life of the bridge. This assumption made it possible to treat the tendons as the only elements, aside from the deck's own flexural stiffness, that govern the vertical displacement of the structure. At this point, the single bridge girder could be modelled as simply supported at its ends and, in place of the tendons, as having intermediate hinges supported by springs with an elastic constant k equal to $\frac{E_{tendons} \cdot A_{tendons}}{L_{tendons}}$.

To analyse the beam for the purposes of this study, the displacement method was adopted. This approach makes it possible to define the stiffness matrix of the structure and to modify only its input parameters, while its overall formulation remains unchanged. As a result, the beam's response to loads can be evaluated efficiently. The method is based on determining the unknown displacements at the various supports of the structure. In the project case, assuming the supports are

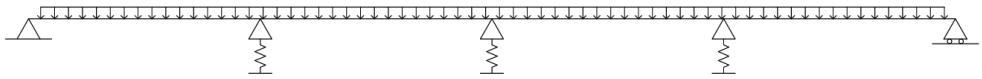

Figure 4.3. Continuous beam supported on springs

numbered from left to right, the unknown displacements are the rotations (ϕ) at the end supports 1 and 5 and the rotations (ϕ) together with the vertical displacements (ν) at the intermediate spring-supported nodes 2, 3, and 4. In total, this leads to eight unknown degrees of freedom. It was therefore possible to identify the following vector of unknown displacements $\{d\}$.

$$\{d\} = \begin{Bmatrix} \phi_1 & \phi_2 & \nu_2 & \phi_3 & \nu_3 & \phi_4 & \nu_4 & \phi_5 \end{Bmatrix}$$

To compute them, the double-clamped diagrams are used for each span of the bridge, and the following conditions are imposed:

- the moment at nodes 1 and 5 is equal to zero;
- the moment at nodes 2, 3 and 4 is equal on both the right and left sides;
- the sum of the shear forces on the right and left of nodes 2, 3 and 4 is equal to the reaction in the spring, i.e. $k_{spring} \cdot \nu$

To obtain the stiffness matrix for each span, the deflections corresponding to the unknown displacements identified in the previous paragraph were applied to the double-clamped beam. This procedure allows the equations associated with the

imposed conditions to be derived; these equations depend directly on the unknown displacements and therefore form the variables of the system. Once the equations were established, an eight-equation system with eight unknowns was obtained. This system can be expressed in matrix form as shown in Equation 4.2.

$$[R] \cdot \{d\} = \{Q\} \tag{4.2}$$

$[R]$ is the stiffness matrix;
$\{d\}$ is the displacements vector;
$\{Q\}$ is the load vector;

The stiffness matrix [R] and the load vector Q are specified below. It can be observed that in matrix [R], as already mentioned above, the elements that are modified in each analysis, due to corrosion, are the beam inertia (I) and the elastic constant (k) of the tendons. This approach allows the input of the matrix to be easily updated at each step of the analysis.

$$\{Q\} = \left\{ -\frac{ql^2}{12} \quad 0 \quad ql \quad 0 \quad ql \quad 0 \quad ql \quad \frac{ql^2}{12} \right\}$$

$$[R] = \begin{bmatrix} \frac{4EI}{l} & \frac{2EI}{l} & \frac{6EI}{l^2} & 0 & 0 & 0 & 0 & 0 \\ \frac{2EI}{l} & \frac{8EI}{l} & 0 & \frac{2EI}{l} & \frac{6EI}{l^2} & 0 & 0 & 0 \\ \frac{6EI}{l^2} & 0 & k_2 + \frac{24EI}{l^3} & -\frac{6EI}{l^2} & -\frac{12EI}{l^3} & 0 & 0 & 0 \\ 0 & \frac{2EI}{l} & -\frac{6EI}{l} & \frac{8EI}{l} & 0 & \frac{2EI}{l} & \frac{6EI}{l^2} & 0 \\ 0 & \frac{6EI}{l^2} & -\frac{12EI}{l^3} & 0 & k_3 + \frac{24EI}{l^3} & -\frac{6EI}{l^2} & -\frac{12EI}{l^3} & 0 \\ 0 & 0 & 0 & \frac{2EI}{l} & -\frac{6EI}{l} & \frac{8EI}{l} & 0 & \frac{2EI}{l} \\ 0 & 0 & 0 & \frac{6EI}{l^2} & -\frac{12EI}{l^3} & 0 & k_3 + \frac{24EI}{l^3} & -\frac{6EI}{l^2} \\ 0 & 0 & 0 & 0 & 0 & \frac{2EI}{l} & -\frac{6EI}{l} & \frac{4EI}{l} \end{bmatrix}$$

It is therefore possible to calculate the unknown displacements by inverting Equation 4.2, obtaining:

$$\{d\} = [R]^{-1} \cdot \{Q\} \tag{4.3}$$

Once the displacements were determined, it became possible to calculate the stresses at the supports and subsequently along the entire structure. All computations were carried out using $MATLAB$.

To advance toward the main objective, it was also necessary to incorporate and evaluate the environmental variables governing the corrosion rate. Based on the models described in the previous sections, the following data had to be identified:

- TOW. Time of wetness, annual fraction of number of hours/year in which RH $> 80\%$ and T > 0 $\circ$C;
- SO_2. Avarage concentration mg/m^3;
- Cl. Deposition rate $mg/m^2.day$;
- T. Air avarage temperature ($^\circ C$);
- RH. Relative Humidity (%).

In Italy, each region has an environmental agency equipped with monitoring stations distributed across the territory to measure the parameters required for corrosion analysis. In Piedmont, this role is fulfilled by ARPA, whose website provides access to hourly measurement data from the various monitoring stations. To determine which ARPA station to use and subsequently compute the environmental variables, it was first necessary to define the hypothetical location of the bridge. The bridge was assumed to be situated in Turin, crossing the River Po, which allowed the identification of nearly all the environmental variables required for the analysis.
The ARPA station that best corresponds to these conditions is "Torino-Vallere" [63]. Using the hourly data downloaded from this station, the average relative humidity and the average annual temperature were calculated. From the same dataset, the Time of Wetness (TOW) was also derived. To determine the annual concentration of SO_2, reference was made to ARPA's annual air-quality report, which provides the corresponding yearly average value [64].

Although chlorides are not typically present in the urban environment of Turin, it was considered that the use of de-icing salts during winter could introduce chloride-contaminated water capable of affecting the structure. Using the guidance provided in BS EN ISO 9223:2012 [65], a plausible value for this parameter was estimated based on the classification table shown in Figure 4.4. Since Turin is not exposed to a highly saline atmosphere, yet may still experience chloride input from winter maintenance operations, class S_1 was adopted as the reference class.

In conclusion, the following average environmental parameters were considered:

- $TOW = 4416\ hrs/year$;
- $SO_2 = 5\ mg/m^3$;
- $Cl = 10\ mg/m^2.day$;
- $T = 15.1\ (°C)$;
- $RH = 69\ (\%)$.

Deposition rate of chloride mg/(m²·d)	**Level**
$S_d \leq 3$	S_0
$3 < S_d \leq 60$	S_1
$60 < S_d \leq 300$	S_2
$300 < S_d \leq 1\,500$	S_3

Figure 4.4. Grouping of pollution by airborne salinity represented by chloride

Considering that the data taken into account are specific to the selected station and are therefore not fully representative, it was decided to perform additional analyses by varying the average environmental parameters obtained. The variation was carried out by fluctuating the values according to a Gaussian distribution around the mean value derived from the ARPA station.

Chapter 5

Case 1: Steel Deck Bridge

As a preliminary analysis, a steel deck configuration consisting of longitudinal and transverse beams with bracing was adopted. Although the transverse beams and bracing were not included in the structural model, they were considered in the load evaluation to ensure that all actions acting on the bridge were accounted for.

Given the relatively short span between adjacent tendons, a commercial steel profile could be used. The longitudinal beam selected was an IPE 550, whose geometric properties are shown in Figure 5.1. The steel grade adopted was S355. In accordance with the NTC 2018 design provisions, the yield strength of the steel was divided by the partial safety factor of 1.05. In addition, the Young's modulus of steel and its density are respectively equal to210 GPa e 78.5 kN/m^3. Consid-

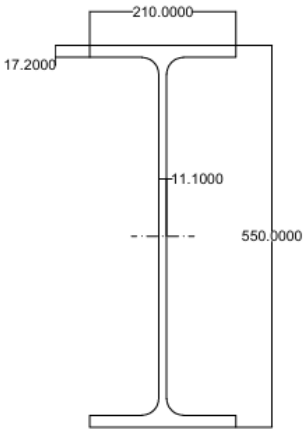

Figure 5.1. IPE 550. Commercial Profile [66]

ering the information described above, the cross-beams were selected as IPE 500

profiles, and the deck section was therefore fully defined (Figure 5.2). With the deck geometry established, it becomes possible to calculate the loads acting on the structure. In particular, each longitudinal beam was assumed to carry the loads distributed over half of the deck width, i.e., 3.5 m. Based on these assumptions, the total load acting on each beam, already including the partial safety coefficients, amounts to 64.63 kN/m.

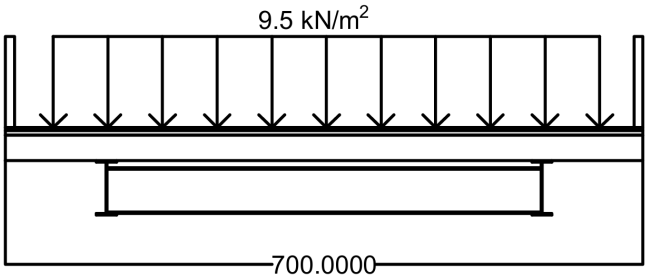

Figure 5.2. Cross-section of the steel bridge

As outlined in the introduction to this chapter, it was then possible to determine the number of strands required for both the tendons and the main cable. The resulting cross-sections are presented below:

- Tendon. 7 strands ($Area = 139\ mm^2$) of 7 wires each , for a total area of 973 mm^2
- Cable. 12 strands ($Area = 139\ mm^2$) of 7 wires each , for a total area of 1700 mm^2

Now that the structure has been fully defined, it was possible to implement the $MATLAB$ model for the structural analysis of the bridge.

To complete the preliminary decisions for the project, it is necessary to identify the model that best represents the corrosion process. For both the carbon-steel beam and the tendons, this choice is relatively straightforward, as only one reliable model has been identified for characterising long-term corrosion. This model incorporates a wide range of environmental variables and is supported by an extensive experimental dataset, making it sufficiently robust for describing the corrosion behaviour of the bridge examined in the case study. By substituting the empirical coefficients presented in the tables in Section 3.2 into Model 3.31, the final formulation used in the analyses is obtained.

$$y = 13.4 \cdot t^{0.98}(\frac{TOW}{3800})^{0.46} \cdot (1 + \frac{S0_2}{25})^{0.62} \cdot (1 + \frac{Cl}{50})^{0.34} \cdot e^{0.016 \cdot (T+20)} \tag{5.1}$$

The steel elements were assumed to be protected by galvanization. In particular, a coating thickness of 100 μm was considered for the beams and 150 μm for the tendons. For the analysis of zinc coating degradation, the same corrosion model was adopted, modifying only the empirical coefficients to account for the specific behaviour of galvanized steel.

$$y = 0.16 \cdot t^{0.36}(\frac{TOW}{3800})^{0.24} \cdot (1 + \frac{S0_2}{25})^{0.82} \cdot (1 + \frac{Cl}{50})^{0.44} \cdot e^{0.05 \cdot (T+20)} \tag{5.2}$$

The decision to adopt a thicker zinc layer for the tendons is motivated by their significantly larger exposed surface area, which results in a higher potential corrosion rate compared with the beams. Furthermore, it is assumed that corrosion of the structural steel begins only once the entire zinc coating has been consumed.

With this information, the analysis of the bridge can begin. First, the preliminary dimensioning of the structure was verified. The figures below show the bending moment (Figure 6.3) and shear stress (Figure 6.4) distributions along the beam, which were compared with the corresponding sectional resistances.

Additionally, the discontinuity observed at the central supports of the beam corresponds precisely to the force carried by the tendons, enabling verification that the tendons are capable of sustaining this tensile load. At the beginning of the bridge's service life, the safety factors (SF) of the various structural components are as follows:

- SF positive moment equal to 1.54
- SF nevative moment equal to 1.20
- SF shear equal to 3.07
- SF tension in tendons equal to 2.16

Once the stability of the bridge had been verified, its behaviour over its service life was analysed by applying corrosion to the structural elements. To achieve this, dedicated functions were developed to progressively reduce the cross-section of both the beams and the tendons. Using a *For* loop, the same structural model was then evaluated year by year, incorporating the corrosion predicted by the selected models.

As discussed in the introduction to this chapter, corrosion depends on environmental parameters that are measured with a certain degree of uncertainty and, in this case, at a specific monitoring location. Moreover, these parameters may

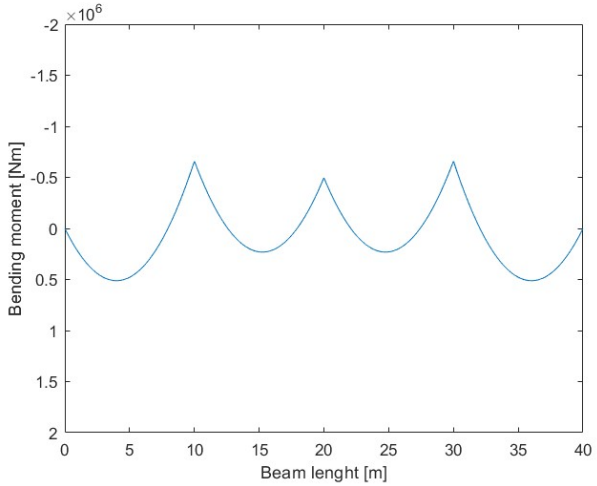

Figure 5.3. Bending moment stress (Nm) on steel bridge girder

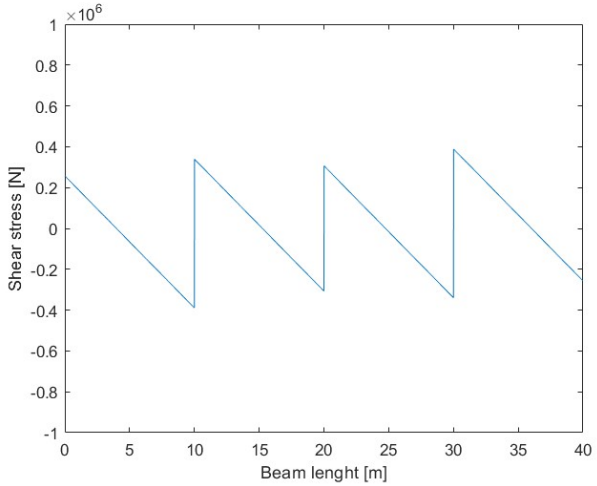

Figure 5.4. Shear stress (N) on steel bridge girder

vary over time, for example, heavier snowfall may lead to increased use of de-icing salts, while rising temperatures associated with climate change may alter humidity or pollutant levels. For this reason, the analysis was repeated multiple times to obtain not a single deterministic estimate of structural failure, but a range of possible outcomes over time. This approach enables more effective planning of maintenance interventions. To introduce variability into the environmental parameters, the $MATLAB$ function $randn()$ was used to modify each parameter

according to $P \cdot (1 + randn \cdot k)$, where k is a coefficient selected based on the type of environmental parameter and its expected range of variation.

5.0.1 Time to failure

This section presents the evolution of the structure's safety factor over time, assuming that no maintenance interventions are carried out. Figure 5.5 illustrates the envelope of the safety factors associated with each type of stress acting on the structural elements, represented in different colours. At each time step, the minimum safety factor among all components is highlighted.

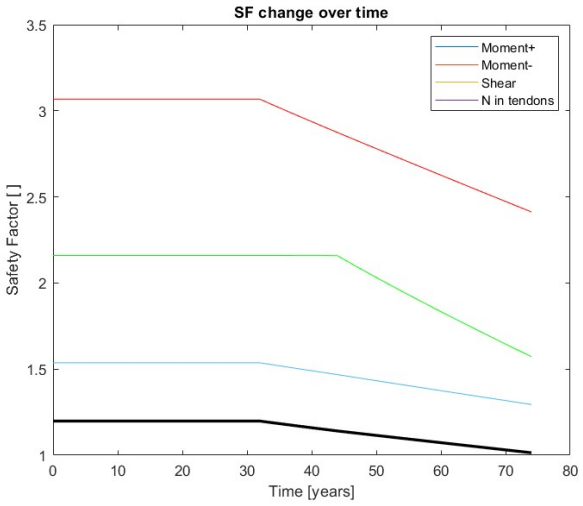

Figure 5.5. Safety Factor of the steel bridge structural element

This visualization helps to clarify the overall structural behaviour and supports the interpretation of the subsequent graphs. In this case, the lowest safety factor consistently corresponds to the negative bending moment, represented by the dark black line in the figure. However, as previously noted, the tendons lose their load-bearing capacity much more rapidly, which is evident from the steeper decline in their safety factor compared with that of the beam. Figure 5.5 illustrates the structural response considering only the individual environmental parameters introduced at the beginning of this chapter. Nevertheless, these parameters are not fully representative on their own, and must therefore be varied repeatedly to obtain a plausible range of outcomes.

Figure 5.6 presents the safety factor (SF) obtained from 20,000 simulations, each

generated by multiplying the environmental parameters by random factors normally distributed around a mean value of 1. Instead of a single deterministic failure time, the result is a distribution of 20,000 values around a mean, providing a more comprehensive and realistic understanding of the potential degradation of the structure.

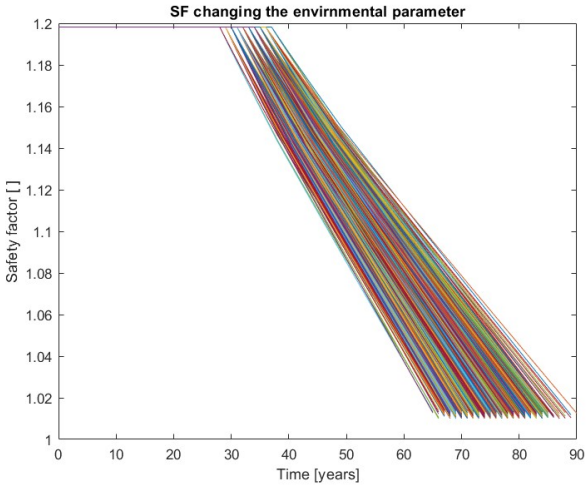

Figure 5.6. Safety Factor of the steel bridge, changing the environmental parameter

This approach is particularly useful for planning maintenance and inspection activities more effectively. Figure 5.7 illustrates the Gaussian distribution of the predicted failure years. Based on this distribution, a maintenance and inspection plan can be developed with the understanding that, around the 68th year of the bridge's service life, corrosion may already be at an advanced stage and could potentially lead to structural failure.

From this analysis, suitable maintenance strategies can be identified. For this project, three approaches were considered:

- reducing the forces acting on the bridge,
- re-galvanizing the structural components, and
- performing an initial repainting followed by reconstruction of the deteriorated sections.

It has been observed that, when designing corrosion protection for structural elements, it is essential to consider the actual cause of structural failure. In Figure 5.8, a structural simulation was performed for two cases: one in which the zinc

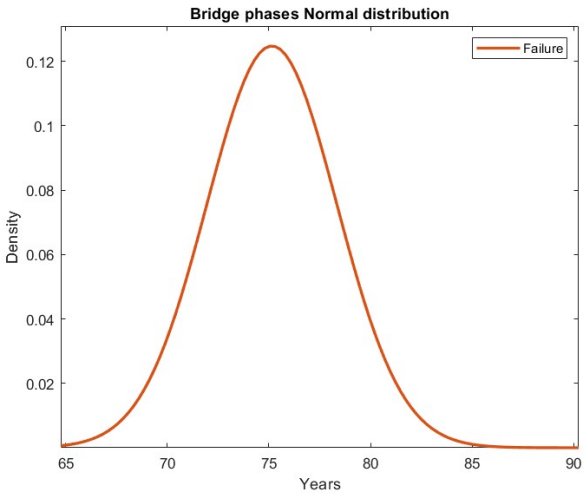

Figure 5.7. Safety Factor of the steel bridge. Normal distribution

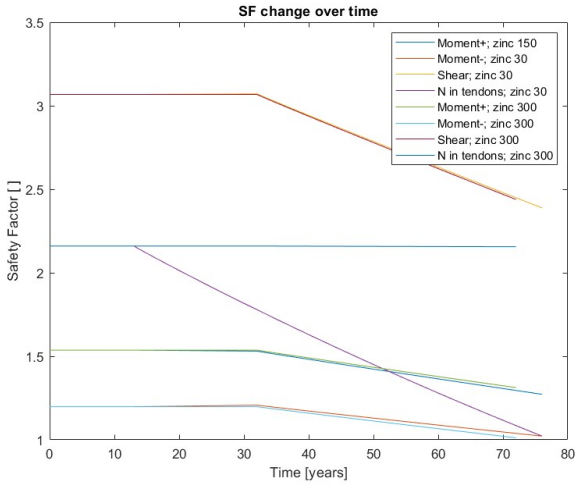

Figure 5.8. Safety Factors of the steel bridge. Comparison between two different thick of protection

coating on the tendons is 300 μm thick and another with a 30 μm coating.

These values were selected to clearly highlight the differences between the two configurations. The initial expectation was that both structures would fail at approximately the same time, since only the tendon protection was modified, or that increasing the protection of a structural element would extend the overall service

life of the bridge. However, the simulation revealed the opposite behaviour: the structure with thinner tendon protection actually exhibited a lifespan more than four years longer. This outcome arises because the failure of the structure with thicker zinc protection is governed by excessive negative bending moments, whereas when the tendons begin to corrode earlier, their stiffness decreases, which in turn reduces the negative moment. This result demonstrates that maintenance strategies must be tailored to each specific structure, as increasing corrosion protection does not necessarily lead to improved long-term performance.

5.0.2 First approach: Load reduction

The first approach tested to extend the life of the bridge was to reduce the applied loads, specifically the variable loads. Initially, the bridge was designed for a 44 *tons* vehicle, corresponding to a distributed load of 9.5 kN/m^2 When the overall safety factor of the structure falls below the limit of 1.02, vehicles exceeding 44 *tons*, , equivalent to a distributed load of 7.5 kN/m^2, are prohibited. If the safety factor drops below the limit again, the allowable load is further reduced, restricting vehicles over 7.5 *tons*, which corresponds to a distributed load of 4.2 kN/m^2 [67]. This approach does not involve direct costs for extending the bridge's service life; however, limiting heavy-vehicle traffic also restricts the movement of goods, potentially affecting the local economy. Figure 5.9 shows the envelope of

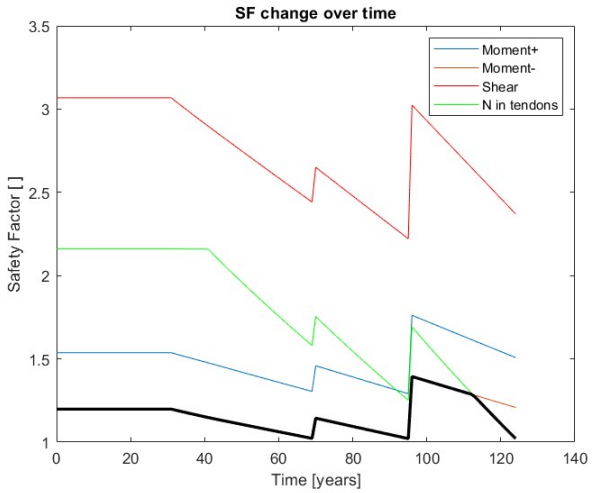

Figure 5.9. Safety Factor of the steel bridge. Approach 1: Load reduction

the safety factors over time, with the minimum safety factor among the four considered stresses, representing the overall structural safety, highlighted in black. The effect of load reduction is clearly visible as an increase in the safety factor.

It can also be observed that, as time progresses, the tendons, whose load-bearing capacity deteriorates more rapidly, become the weakest elements of the bridge, ultimately governing its failure.

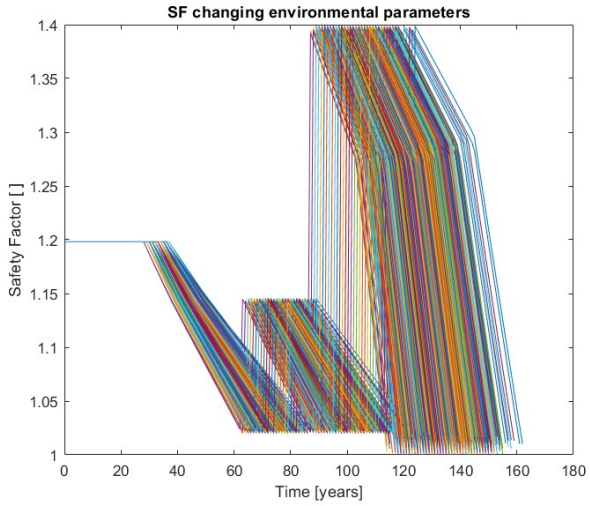

Figure 5.10. Safety Factor of the steel bridge, changing the environmental paarameter. Approach 1: Load reduction

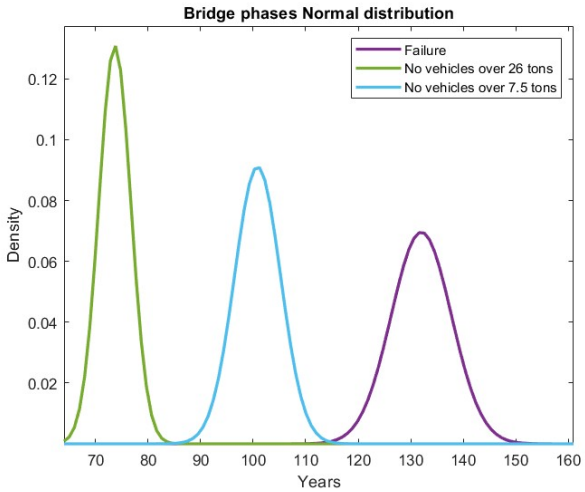

Figure 5.11. Safety Factor of the steel bridge. Normal distributions. Approach 1: Load reduction

Figure 5.10 shows the envelope of the overall safety factor, obtained from 20,000 simulations with varying environmental parameters. The normal distribution of the years in which load reductions occur and the corresponding failure times is presented in Figure 5.11. This information enables decision-makers to identify the most appropriate moments to restrict traffic on the bridge throughout its service life.

It can also be observed that this approach may extend the bridge's service life to as much as 150 years in the most favourable scenario, with an average extension of approximately 135 years. By comparing Figures 5.11 and 5.7, it becomes clear that reducing loads can prolong the bridge's life by at least 60 years.

5.0.3 Second approach: Repainting structural elements

The second maintenance approach considered is cleaning the surfaces of the structural elements and applying a new zinc coating. Specifically, based on the results presented in Section 5.0.1, it was decided to re-galvanize the beams with a thickness of 150 μm and the tendons with 100 μm. Maintenance on the beams is scheduled when their safety factor falls below 1.1, while a threshold of 1.2 is set for the tendons. Figure 5.12 shows the graph of the safety factors calculated for the structural stresses, with the lowest of the four safety factors highlighted in dark black.

As with the previous analyses, 20,000 simulations were carried out in this case

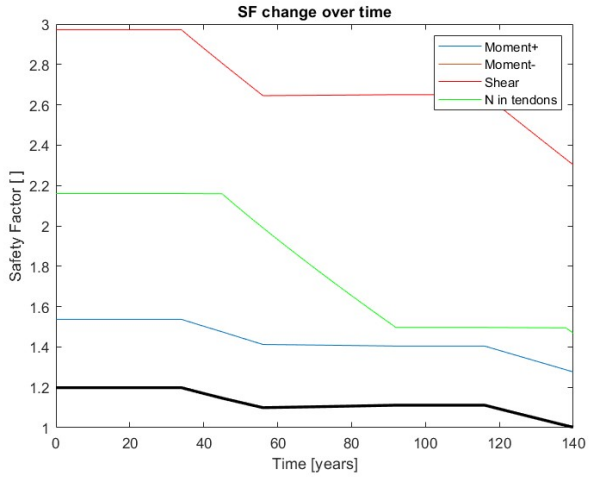

Figure 5.12. Safety Factor of the steel bridge. Approach 2: Repainting structural elements

as well, varying the environmental parameters. Figure 5.13 shows that when the beam is maintained, its safety factor increases. However, the tendons continue to deteriorate and lose stiffness over time, leading to a progressive change in the structural behaviour. As the central supports become less effective, the beam gradually begins to behave more like a simply supported span over the full 40 m length. Consequently, the negative bending moment decreases more rapidly than the reduction in the beam's resistant moment.

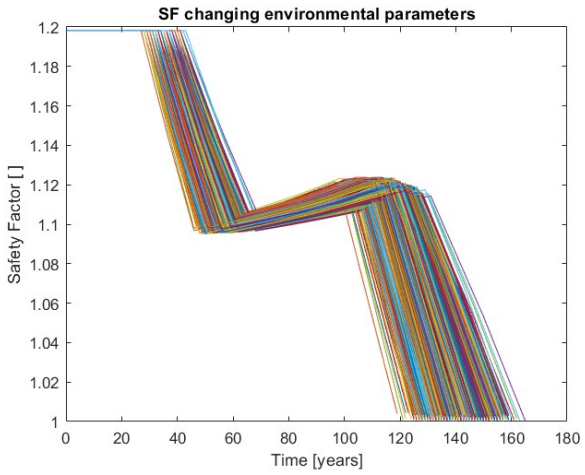

Figure 5.13. Safety Factor of the steel bridge, changing the environmental parameter. Approach 2: Repainting structural elements

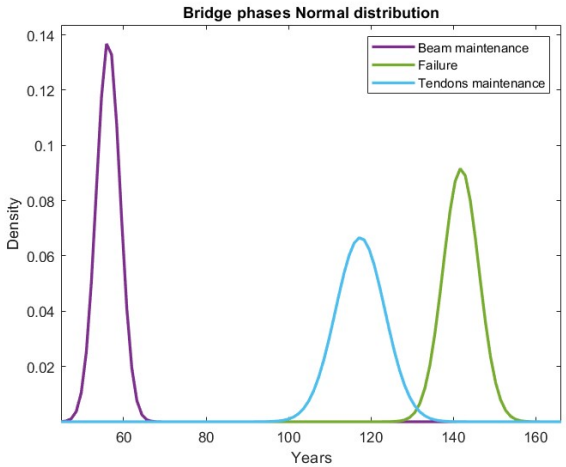

Figure 5.14. Safety Factor of the steel bridge. Normal distributions. Approach 2: Repainting structural elements

Figure 5.14 shows the Normal distributions of the times at which maintenance could be performed for both the beam and the tendons.

It is interesting to note that, in general, the longer the service life of the bridge, the more challenging it becomes to make informed maintenance decisions. This is because the variance of the normal distributions associated with each phase increases over time. However, when maintenance operations or structural failure involve different components of the bridge, this trend does not necessarily hold. As shown in Figure 5.16, the distribution associated with the tendons exhibits a greater variance than the one corresponding to failure on the beam side.

It can also be observed that maintenance of the tendons occurs very close to the point of structural failure. Therefore, performing tendon maintenance earlier may be advantageous, as it could potentially extend the overall service life of the structure. In the figures below, the analysis is repeated with adjusted safety factors and maintenance thresholds. The safety factor for the beam is kept at 1.1, while the safety factor for the tendons is increased to 1.4.

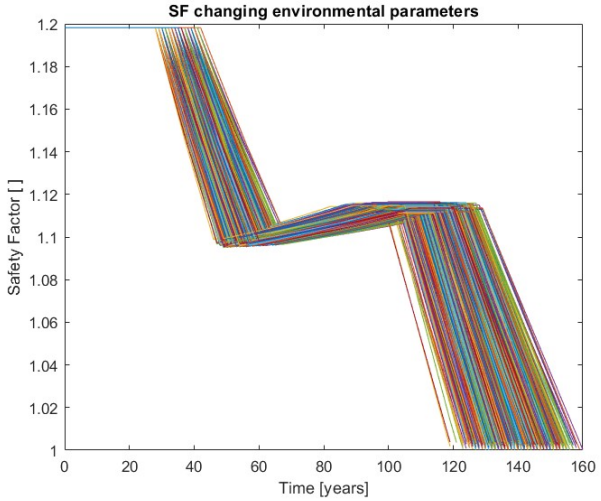

Figure 5.15. Safety Factor of the steel bridge structural element. SF tendons equal to 1.4 . Approach 2: Repainting structural elements

Figure 5.15 shows that, unlike Figure 5.13, the safety factor increases to a lesser extent and then reaches a stable plateau. This behaviour results from the early maintenance of the tendons, which effectively halts corrosion and stabilises the structural response.

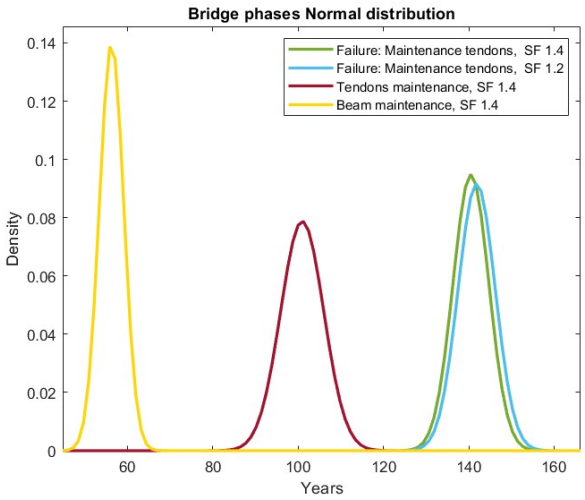

Figure 5.16. Safety Factor of the steel bridge structural element. Gaussian distributions. Approach 2: Repainting structural elements

In Figure 5.16, it can be observed that altering the timing of maintenance does not significantly affect the overall service life of the bridge. However, performing maintenance on the tendons at a later stage allows for a slight extension of the bridge's lifespan. This finding is consistent with the observations presented in Section 5.0.1: as shown in Figure 5.5, tendon maintenance is not fully exploited during the bridge's life, leading to a greater reduction in tendon stiffness, increased deflection, and consequently a larger decrease in the negative bending moment. This once again demonstrates how predictive maintenance, when combined with a thorough structural assessment, can achieve outcomes that may not be attainable through conventional maintenance strategies.

5.0.4 Third approach: Reconstruction of structural elements

The third approach involves re-galvanizing the structural elements when the safety factor falls below 1.1 for both the beam and the tendons, followed by reconstruction of the section once the safety factor reaches 1. The objective is not to replace the beams entirely, but rather to rebuild only the damaged portion until the section recovers its original mechanical properties. After this intervention, the section is allowed to corrode naturally until the structure ultimately reaches failure.

Figure 5.17 presents the envelopes of the safety factors for the stresses analysed

in the structural elements, with the overall structural safety factor highlighted in dark black.

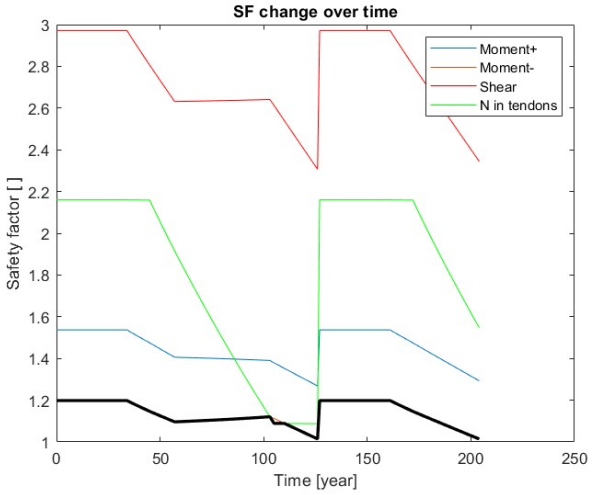

Figure 5.17. Safety Factor of the steel bridge structural element. Approach 3: Reconstruction of structural elements

For this approach as well, the environmental parameters were varied to obtain a range of years during which maintenance should be performed on the different structural elements. Figure 5.18 presents the results of 20,000 analyses, accounting for variations in the parameters governing the degradation models.

In Figure 5.19, the normal distributions representing the years in which maintenance may be required indicate that performing maintenance on the tendons at that specific time may not be the optimal choice. In fact, it may be possible to forgo tendon maintenance altogether and instead advance the general repair of the bridge by a few years.

Figure 5.20 shows the normal distributions of the bridge's failure times, both with and without tendon maintenance. As expected, neglecting tendon maintenance reduces the bridge's service life; however, this is not necessarily the less favourable option. A cost analysis is required to determine whether avoiding tendon maintenance represents a more cost-effective decision.

5.0.5 Cost analysis

To carry out the cost analysis, as mentioned in previous chapters, the prices listed in the regional price list of the Piedmont Region were used. The cost assessment was prepared using Primus, a software developed by ACCA.

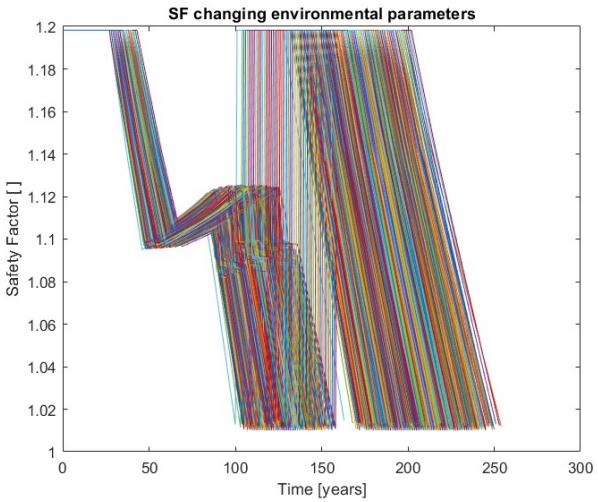

Figure 5.18. Safety Factor of the steel bridge structural element, changing the environmental parameter. Approach 3: Reconstruction of structural elements

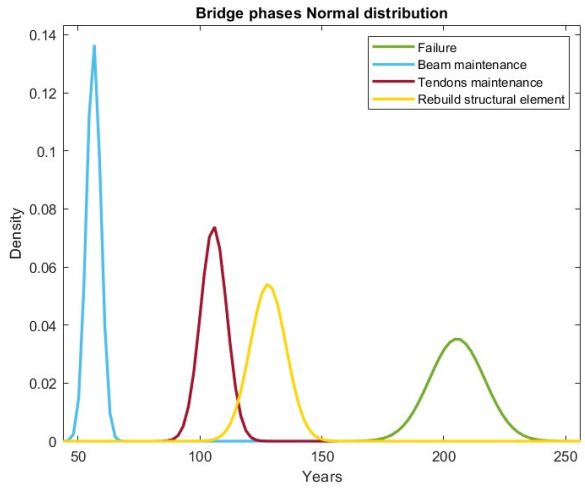

Figure 5.19. Safety Factor of the steel bridge, Gaussian distribution. Approach 3: Reconstruction of structural elements

The costs associated with maintaining the bridge were distributed over a 20-year period, applying an interest rate of 4%, with the condition that the depreciation periods of the various maintenance interventions do not overlap. This prevents excessive simultaneous cash outflows.

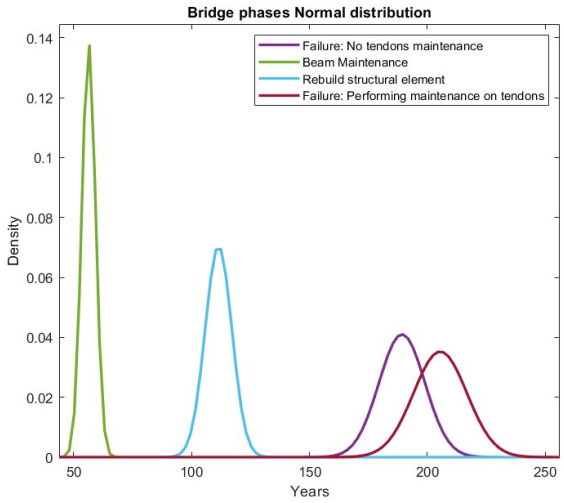

Figure 5.20. Safety Factor of the steel bridge, Gaussian distributions. Approach 3: Reconstruction of structural elements, without tendons repainting

To determine which solution is the most cost-effective, the impact of each maintenance strategy on the service life of the bridge was evaluated. Specifically, the difference between the average failure year after maintenance and the average failure year without maintenance was calculated. The most advantageous solution is considered to be the one with the lowest ratio between the total amount to be repaid, including interest, and the corresponding extension of the bridge's service life.

To obtain results that are as realistic as possible, the costs include not only the direct interventions on the bridge but also expenses related to worksite safety and external interference. As mentioned earlier, it is not possible to perform a cost analysis for the first approach, as this strategy does not involve direct maintenance costs. Instead, it generates an indirect economic impact due to the reduced passage of freight vehicles.

Approach 2: Repainting structural elements

To carry out the repainting works, a total duration of 2 months was assumed for the beams and 1 month for the tendons and the main cable. Based on the results obtained, maintenance of the beams is performed at year 68, while the tendons and main cables are repainted at year 100. The bridge is assumed to reach failure at year 141. Considering that, without any maintenance, the bridge would collapse at year 89, this maintenance strategy increases the service life of the structure by 52 years.

To execute the maintenance on the beams, it was decided to intervene on one beam at a time, allowing the other lane to remain open to traffic. The primary costs associated with these operations are:

- sandblasting and repainting (Figure 5.21) at a cost of 89.56 €, which, having been calculated without the use of the price list, it was decided to add 25% of the cost to consider the profit margin of the person winning the contract;
- multidirectional scaffolding with suspended starting is used to be able to carry out the work with ease.

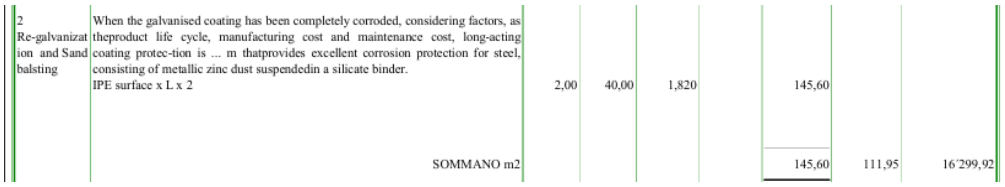

2 Re-galvanization and Sandbalsting	When the galvanised coating has been completely corroded, considering factors, as theproduct life cycle, manufacturing cost and maintenance cost, long-acting coating protec-tion is ... m thatprovides excellent corrosion protection for steel, consisting of metallic zinc dust suspendedin a silicate binder. IPE surface x L x 2	2,00	40,00	1,820	145,60		
	SOMMANO m2				145,60	111,95	16'299,92

Figure 5.21. Example of an item in the bill of quantities

The secondary costs identified are:

- New Jersey type barriers for division from the other lane;
- a traffic light for traffic management;
- a construction site box and a portable toilet;
- metal nets which serve to delimit the construction site area with an attached materials storage area;
- road signs and signal lights

The total cost for two months of work for repainting the beams is 27122.46 €.

The maintenance costs for the tendons are very similar, but reduced to a duration of one month. In this case, multidirectional tubular scaffolding is not required; instead, self-lifting scaffolding is used, which allows work to be carried out at heights of up to 27 m, making it fully suitable for this application. The expected cost for this maintenance activity is 14610.48 €.

To calculate the savings for the contractor responsible for the works, it was assumed that the instalments to be repaid remain constant over the 20-year depreciation

period, and that the bridge has no residual value at the end of its service life. Based on these assumptions, it is possible to compute the annual saving for the contracting authority, which is equal to:

$$AS = TC \cdot \frac{IR \cdot (1 + IR)^Y}{(1 + IR)^Y - 1} \tag{5.3}$$

where:
AS: annual savings;
IR: interest rate;
Y: years in which the debt must be repaid.

By applying this formula, it is possible to calculate the annual payment that must be made to finance the works. In this case, for the maintenance of the steel section, 1995.72€ must be paid per year, while for the maintenance of all the cables, the annual payment is 1075.07€ must be returned annually. Using these values, the total cost required to carry out all the maintenance operations amounts to 61415,66€. Since, as previously discussed, this maintenance approach increases the service life of the structure by 52 years, we can conclude that the cost of extending the bridge's life by one year is 1181.07€.

Third approach: Reconstruction of structural elements

To carry out all the works required for this approach, the repainting operations were considered identical to those described in the previous section. Conversely, for the reconstruction of the section, it was assumed that the duration of the works would be 4 months, 2 months per carriageway, so that at least one lane remains open at all times.

To calculate the years of service life gained with this approach, the two case studies described in Section 5.0.4 were considered. In the first case study, repainting of the beam is performed at 57 years, repainting of the tendons at 105 years, and reconstruction of the steel section at 127 years; the bridge is then allowed to reach collapse at 205 years. In the second case study, maintenance of the tendons is not performed midway through the bridge's life; instead, the general repair is carried out at 111 years, after which the bridge is left to deteriorate naturally, reaching failure at 189 years. In the first case, the resulting extension of service life is 116 years, while in the second case it is 100 years.

The direct costs of reconstructing the sections are as follows, in chronological order:

- the use of scaffolding that develops above and below the roadway;

- sandblasting to remove wrinkles and clean up beam and tendons surfaces;
- assembly of sheet metal of design thickness through the use of welds and bolting to replace the section lost due to corrosion;
- use of strands to reconstitute the section lost due to corrosion.

The indirect costs are very similar to those described for repainting alone, but increased by an additional 2 months. Based on these considerations, the total cost for repairing the load-bearing sections of the bridge was calculated to be 68,886.06 €.

To calculate the depreciation of this cost, the formula in Equation 5.3 was applied again, assuming constant annual payments over a 20-year period and an interest rate of 4%. Using this approach, the annual payment required to cover the repair of the sections is 5068.77€. The total costs, including interest, amount to 162,790.79 € when the tendons are also repainted, and 141,289.50 € when tendon maintenance is omitted. Knowing the expected service life of the bridge for each scenario, the cost per additional year of life can be calculated: 1403,371€ per year for the first case and 1412,89€ per year for the second case.

These results allow for more informed decision-making. In fact, Approach 2 (repainting alone) costs 1181.07€ per additional year of bridge life, which is nearly 300€ less per year compared with the reconstruction options described above. Furthermore, it is technically simpler, as it avoids the need to reconstruct the load-bearing sections of the structure.

Chapter 6

Case 2: Concrete Deck Bridge

To analyse the behaviour of concrete within this project, the same bridge was also designed using this material. The deck consists of two longitudinal beams connected by transverse beams. Although the transverse beams were not included in the structural model, they were considered in the load evaluation to ensure that all actions acting on the bridge were accounted for.

An element height of 700 mm was adopted, with a concrete cover of 50 mm. The amount of reinforcement required for the concrete section was then estimated, assuming that the section operates in field 3 with respect to the stress state. Following a preliminary structural analysis, it was also possible to evaluate the shear stresses within the structure and, consequently, to propose the presence of transverse reinforcement. The reinforcement provided is as follows:

- Lower part reinforcement. 11 ϕ20.
- Upper part reinforcement. 13 ϕ20.
- Stirrups. 1 ϕ6 each 10 cm

The geometric dimensions of a single span (10 m) are shown in Figure 6.1. The concrete used is class C30/37, while the reinforcement steel is C 30/37. The safety coefficients proposed by NTC 2018 were used for the design. Therefore, the characteristic compressive strength of the concrete was divided by the partial safety coefficient of 1.5 and multiplied by 0.85, while the characteristic strength of the reinforcing steel was divided by 1.15. In addition, the Young's modulus and density of the reinforcing steel are equal to 210 GPa e 78.5 kN/m^3 respectively, while the Young's modulus and density of the concrete are equal to 30 GPa e 24

kN/m^3, respectively. The Young's modulus values were used to obtain the homogenised moment of inertia of the section. In particular, the steel reinforcement was transformed into an equivalent concrete area. The homogenisation coefficient was assumed equal to 7.

With this in mind, the cross-section has been fully defined, as shown in Figure

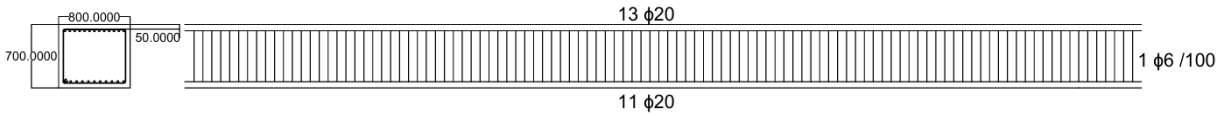

Figure 6.1. Concrete bridge section

6.2. Based on these data, it is possible to calculate the load acting on a single beam, to which 3.5 m of the deck are tributary. The total load acting on each beam is therefore equal to 79.32 kN/m As described in the introduction to this

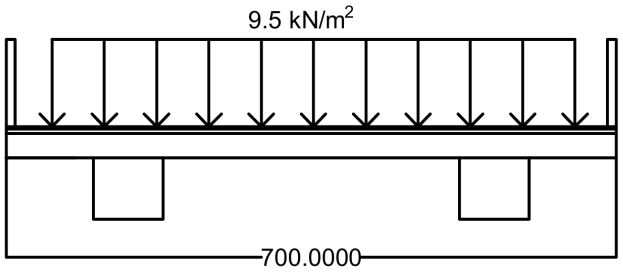

Figure 6.2. Cross-section of the reinforced concrete bridge

chapter, it was then possible to determine the number of strands required for both the tendons and the main cable. Based on the load assumptions and the tensile resistance of the individual strands, the following cross-sections were identified:

- Tendon. 8 strands ($Area = 139\ mm^2$) of 7 wires each , for a total area of 1100 mm^2
- Cable. 14 strands ($Area = 139\ mm^2$) of 7 wires each , for a total area of 1900 mm^2

Now that the structure has been fully defined, the MATLAB model for the structural analysis of the bridge could be developed. Since the inertia modulus is homogenised, the elastic modulus adopted in the analysis is that of concrete, as the steel area has been transformed and homogenised with respect to the concrete material.

The next step was to select an appropriate model to evaluate degradation over time. Because the bridge is assumed to be located in Turin, carbonation was considered the governing degradation mechanism. If the bridge were situated in an area with higher chloride concentrations, it would be necessary to verify whether carbonation or chloride diffusion controls the deterioration process. For simplicity, the carbonation rate was evaluated using Model 3.6, which depends solely on time and requires only the water-to-cement ratio as input. A water-to-cement ratio of 0.4 was adopted; therefore, the model used in the analyses can be expressed as:

$$x = -0.56213 - \frac{8.792}{\sqrt{t}} + 17.8372(d_c) \tag{6.1}$$

For reinforcement corrosion, Model3.16 was adopted. Relative humidity and temperature were environmental parameters that could be readily obtained, whereas the chloride content could not be directly evaluated. For this reason, the chloride concentration was assumed to be constant and conservatively set to 0.43 %, corresponding to the maximum value permitted by the model. The corrosion-rate expression can therefore be written as follows:

$$i_{corr}(t) = 2.486 \cdot (\frac{RH}{45})^{1.6072} \cdot (\frac{T}{10})^{0.3879} \cdot (\frac{w/c}{0.35})^{0.4447} \cdot (\frac{d_c}{10})^{-0.2761} \cdot 0.43^{1.7376} \tag{6.2}$$

For this part of the analysis, a pitting coefficient equal to 4 was adopted. This choice is consistent with the assumption of carbonation-induced corrosion, which typically results in relatively uniform corrosion along the reinforcement. At the same time, the selected value allows for a minimal level of local imperfections within the bars, which may give rise to limited pitting effects.

$$P_x = 0.0116 \cdot i_{corr} \cdot t_p \cdot \alpha \tag{6.3}$$

where:
P_x : is the diameter loss (mm);

The model used directly calculates the loss of rebar diameter over the corrosion period, unlike the carbon-steel and tendon models, which instead focus on the reduction of thickness.

Corrosion of the rebars is assumed to begin once the entire concrete cover has carbonated. For the tendons, the corrosion process is treated as described in Section5, with the exception that the galvanization thickness has been reduced to 100 μm.

Before proceeding with the degradation analysis, the preliminary structural design was verified. The figures below show the bending moment (Figure 6.3) and shear stress (Figure 6.4) distributions along the beam, which were compared with the corresponding sectional capacities. In addition, the displacement at the central supports of the beam matches the force acting in the tendons, confirming that the tendons are capable of safely resisting the induced tension.

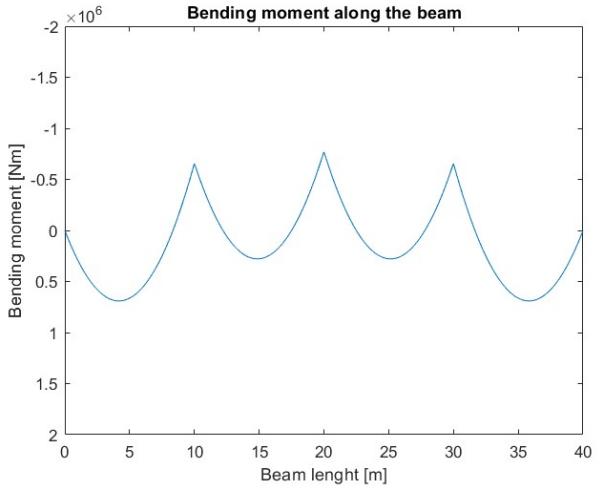

Figure 6.3. Bending moment stress (Nm) on concrete bridge girder

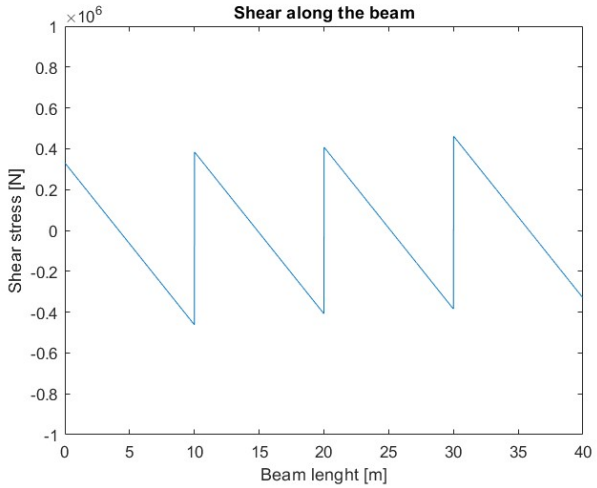

Figure 6.4. Shear stress (N) on concrete bridge girder

At the beginning of the bridge's life, the safety factors (SF) of the various

structural parts are:

- SF positive moment equal to 1.14
- SF nevative moment equal to 1.21
- SF shear equal to 1.76
- SF tension in tendons equal to 2.12

The degradation of the structural elements was then introduced into the model. Specific functions were created to progressively reduce the cross-section of the concrete and the tendons. Subsequently, by using a *For* loop, the same structural model could be reused while applying the degradation calculated by the models year by year.

The carbonation model is relatively simple, depending only on the water-to-cement ratio and the concrete cover, which may vary slightly on site. The reinforcement corrosion model, by contrast, depends on environmental parameters and other factors subject to uncertainty. To account for these variations, multiple simulations were performed to obtain not just a single estimate of structural failure, but a range of possible outcomes over time. This approach provides a clearer understanding of when maintenance is likely to be required and how it should be planned. In MATLAB, the $randn()$ function was used to modify each parameter slightly as $1 + randn * k$, where k is determined based on the type of data and its possible range of variation.

6.0.1 Time to failure

This section evaluates the time to structural collapse, defined as the point at which the safety factor of the bridge reaches 1. Figure 6.5 shows the envelopes of the safety factors for all structural elements under the stresses considered. The overall safety factor of the structure, corresponding to the minimum safety factor among all elements, is highlighted in black.

Initially, an investigation was carried out to determine whether this decrease was caused by a greater relative corrosion of the lower and upper reinforcement bars, by a more pronounced increase in the negative bending moment compared with the positive moment, or by a combination of both effects. It was verified that, as a result of reinforcement corrosion, the ratio between the areas of the reinforcement bars remains constant. However, the ratio between the maximum negative moment and the maximum positive moment increases over time. This behaviour is primarily attributable to the corrosion of the tendons and to the structural response

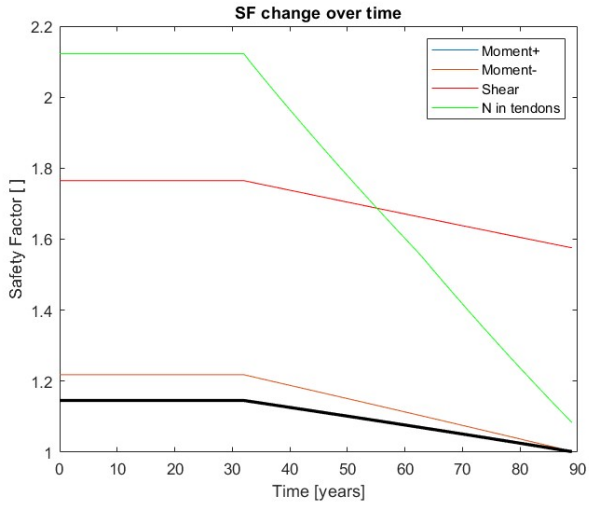

Figure 6.5. Safety Factor of the concrete structural element

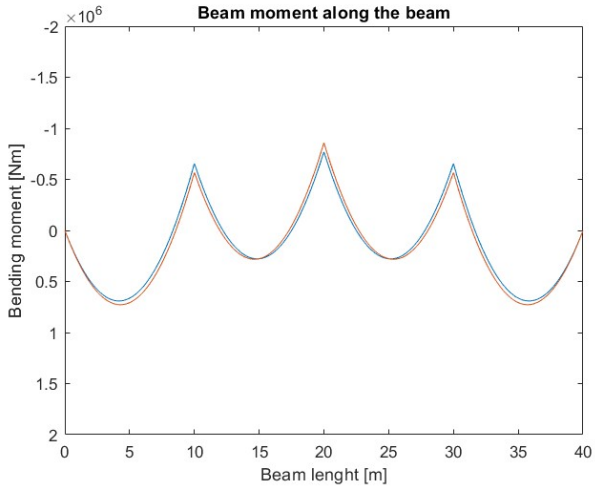

Figure 6.6. Comparison between Bending moment stress (Nm) on concrete bridge girder

characteristic of this type of bridge. Figure 6.6 compares the bending-moment diagrams for the first and last years of the bridge's service life. It can be observed that the negative moment increases at the central support and decreases at the two lateral supports, while the positive moment exhibits the opposite trend. This difference is likely linked to the corrosion models: concrete, which deteriorates more slowly, is able to preserve conditions closer to the initial state for a longer

period.

The figures below show the results of the analyses performed by varying both environmental and material parameters. As illustrated in Figure 6.7, the structural response differs across simulations. This variability arises because changes in certain material-related parameters partially modify the resistance of the structural elements, thereby influencing the overall behaviour of the bridge and the predicted time to failure.

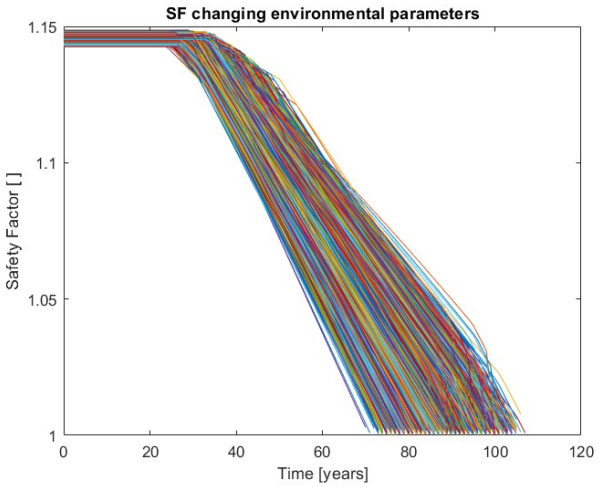

Figure 6.7. Safety Factor of the steel bridge, changing parameter

Furthermore in the Figure 6.8 the normal distributions of the year of collapse of the concrete and steel bridge. Naturally, the two structures differ, and therefore the predicted year of collapse also varies. What is particularly noteworthy, however, is the variance of the two distributions. The variance for the steel structure is 13.01 years, whereas for the concrete structure it reaches 22.29 years. This difference arises because, in addition to environmental parameters, the material parameters of the concrete structure are also varied. Even small fluctuations in these parameters lead to a much wider dispersion of results, highlighting that, from a corrosion-related perspective, concrete structures exhibit a more unpredictable behaviour than steel structures.

To prevent structural failure, the same maintenance strategies adopted for the steel bridge were applied to the concrete bridge. The first approach consists of reducing heavy-vehicle traffic by restricting vehicles exceeding 26*tons* and, subsequently, those exceeding 7.5 *tons*. The second approach involves resurfacing the

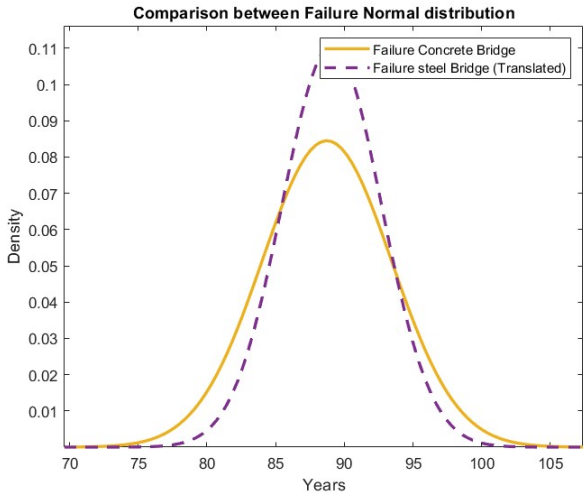

Figure 6.8. Comparison between the year of collapse of the steel structure and the concrete structure

concrete cover to restore uncarbonated concrete and inhibit corrosion, potentially through the use of corrosion inhibitors. The third approach consists of performing maintenance at approximately half of the structure's service life, as in the second approach, followed by reconstruction of the section through reconstitution of the corroded portion.

6.0.2 First approach: Load reduction

The first approach, as already explained, involves reducing the forces acting on the structure, in particular the variable forces due to traffic. At the beginning of the bridge's life, 44 *tons* vehicles are allowed to pass, resulting in a distributed load of 9.5 kN/m^2. When traffic restrictions are introduced, the distributed variable load is first reduced to 6.5 kN/m^2 and then further reduced to 4.2 kN/m^2 .

Figure 6.9 shows the envelope of the safety factors of the structural elements analysed under the different stress conditions. It is evident that the strands experience a faster corrosion rate and, although they initially exhibit a higher safety factor, the structure ultimately fails due to tendon deterioration. Furthermore, it can be observed that, for the beam section, the safety factor associated with the negative bending moment decreases more rapidly over time.

In the following images, the graphs obtained from the analyses performed by varying the environmental and material parameters are shown. In Figure 6.11, it can

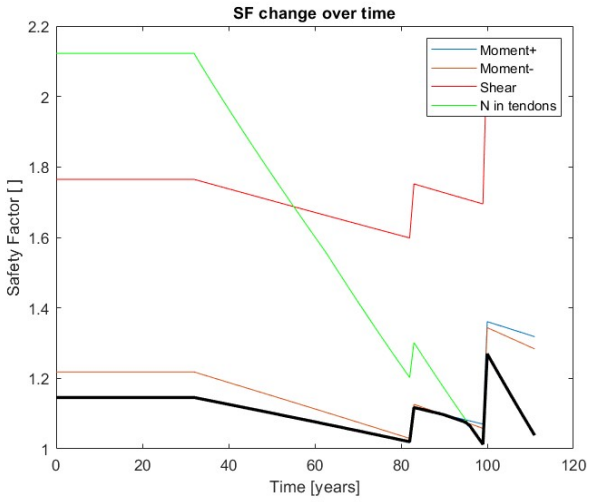

Figure 6.9. Safety Factor of the concrete bridge. Approach 1: Load reduction

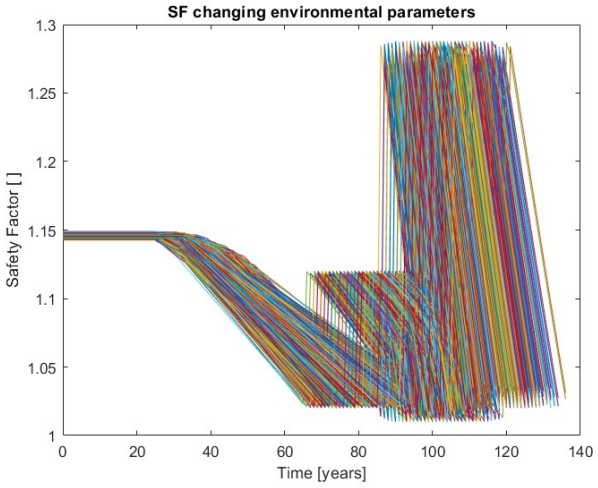

Figure 6.10. Safety Factor of the concrete bridge, changing the environmental parameter. Approach 1: Load reduction

be observed that the different scenarios overlap across very wide ranges. This indicates that the behaviour of concrete structures is more difficult to predict and may therefore require more frequent inspections compared with steel bridges.

Additionally, the figures show that, given the corrosion rate of the tendons, the reductions in applied loads occur within a relatively narrow time interval. As a

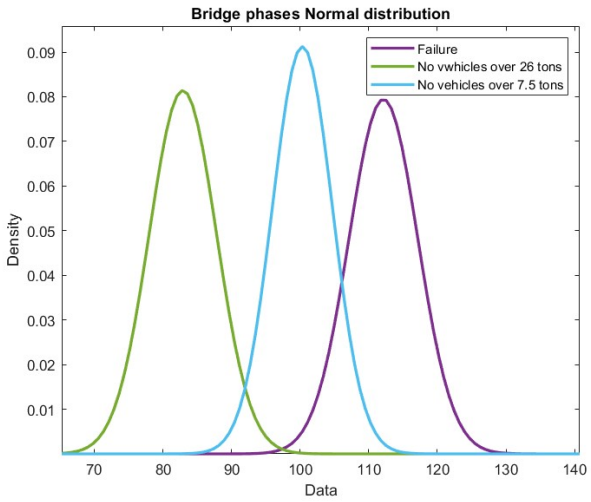

Figure 6.11. Safety Factor of the concrete bridge. Gaussian distributions. Approach 1: Load reduction

consequence, it is not possible to significantly extend the service life of the structure: implementing load-reduction measures increases the bridge's lifetime by only approximately 40 years.

6.0.3 Second approach: Repair structural elements

The second approach consists of performing maintenance on the structural elements at a specific point during the service life of the bridge and then allowing the structure to reach failure naturally. In particular, maintenance on the concrete beams is scheduled when the safety factor decreases to 1.1. This intervention involves removing the carbonated concrete, applying corrosion inhibitors where appropriate to slow or halt the corrosion process, and subsequently reconstructing the removed concrete layer. For the tendons, maintenance is planned when the safety factor reaches 1.3. This operation entails removing the two outer protective layers, repainting the surface, and reapplying the protective layers to restore the original protection system.

Figure 6.12 illustrates the response of the analysed structural elements in terms of the safety factors associated with the considered stress states. It can be observed that, when maintenance is carried out on the concrete beam cross-section, the decrease in the safety factor becomes slower. However, it is evident that the corrosion of the tendons has a greater influence on the negative bending moment. Moreover, it can be observed that maintenance performed on the tendons also

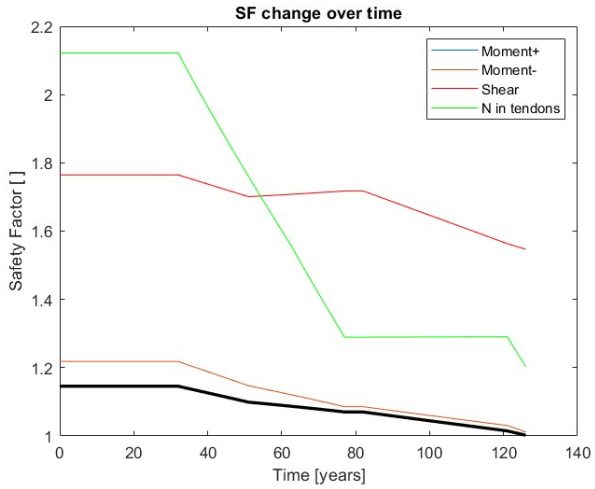

Figure 6.12. Safety Factor of the concrete bridge. Approach 2: Repair structural elements

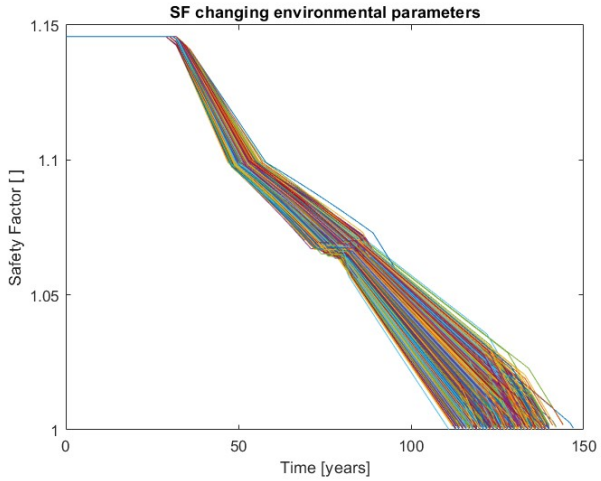

Figure 6.13. Safety Factor of the steel concrete, changing the environmental parameter. Approach 2: Repair structural elements

influences the behaviour of the beam: once the tendons are maintained, the safety factor of the beam remains nearly constant over time. Conversely, maintenance of the beam does not affect the tendons, whose safety factor remains unchanged while the beam continues to deteriorate.

Figure 6.13 presents the results of the analyses carried out by varying the environmental parameters. Consistent with the findings obtained for the steel bridge, Figure 6.14 shows that the interval between maintenance operations is appropriate, allowing all proposed strategies to be implemented effectively.
Considering the results obtained, it was decided to investigate whether performing

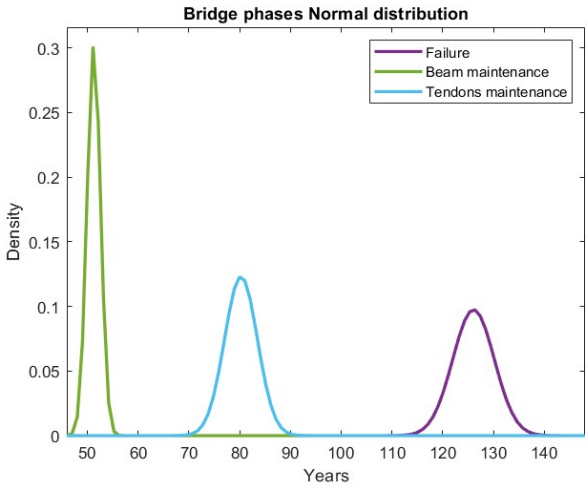

Figure 6.14. Safety Factor of the concrete bridge. Gaussian distributions. Approach 2: Repair structural elements

maintenance at different safety-factor threshold values influences the final outcome. In simple terms, the objective is to determine whether carrying out maintenance at one stage of the bridge's service life is more effective than at another. To this end, 10,000 simulations were performed by randomly varying, within the previously defined limits, the safety factors at which maintenance is triggered.

The first test involved randomising the safety-factor thresholds while imposing a lower bound of 1.01 for both structural elements. If the randomisation produced a value below 1.01, MATLAB automatically assigned 1.01 as the threshold. The results of this analysis are shown in Figure 6.15. The 10,000 outcomes are tightly clustered around an average service life of approximately 127 years. However, it was observed that in cases where failure did not occur at around 127 years, one or both of the maintained elements did not fully benefit from the maintenance intervention. This occurred because structural failure took place before the reconstructed concrete had fully carbonated or before the zinc coating around the tendons had completely corroded.

For this reason, the limit safety factors were increased. Specifically, a threshold of

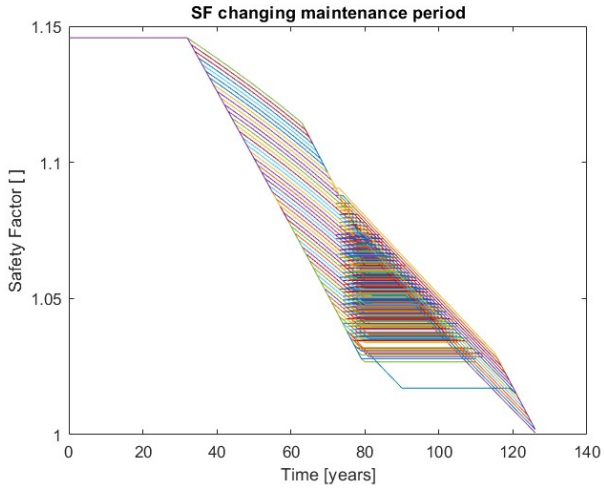

Figure 6.15. Safety Factor of the concrete bridge. Randomizing the safety factors. Approach 2: Repair structural elements

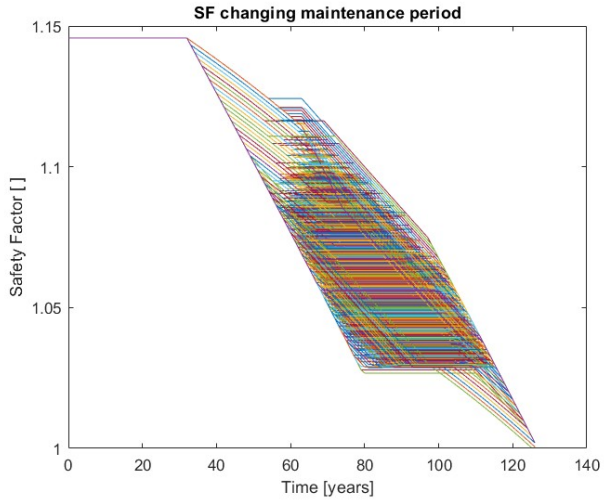

Figure 6.16. Safety Factor of the concrete bridge. Randomizing the safety factors. Approach 2: Repair structural elements

1.03 was set for the concrete elements and 1.25 for the tendons. These limits were introduced to ensure that both elements fully benefit from the protection restored during maintenance. Figure 6.16 shows the results of the new analysis, in which the safety-factor thresholds were randomised. As expected, when the galvanisation is fully corroded and the concrete is completely carbonated, all analysed cases converge to the same failure year, equal to 127 years.

This result allows us to conclude that, in this case, the precise timing of maintenance on the two structural elements is not particularly critical. What truly matters is that maintenance is performed in such a way that the protection provided by each intervention is fully utilised. Consequently, the principle of overlapping effects can be applied. To clarify this concept, Figure 6.17 illustrates all possible combinations that may occur during the service life of the bridge: a phase in which both elements are protected, a phase in which only one element is protected, a phase in which only the other element is protected, and finally a phase in which neither element is protected. Figure 6.18 provides several examples to further illustrate this behaviour.

To achieve a condition in which maintenance on the elements can be performed at any desired time, the following equality must be satisfied:

$$tan(\alpha) + tan(\beta) = tan(\gamma) \tag{6.4}$$

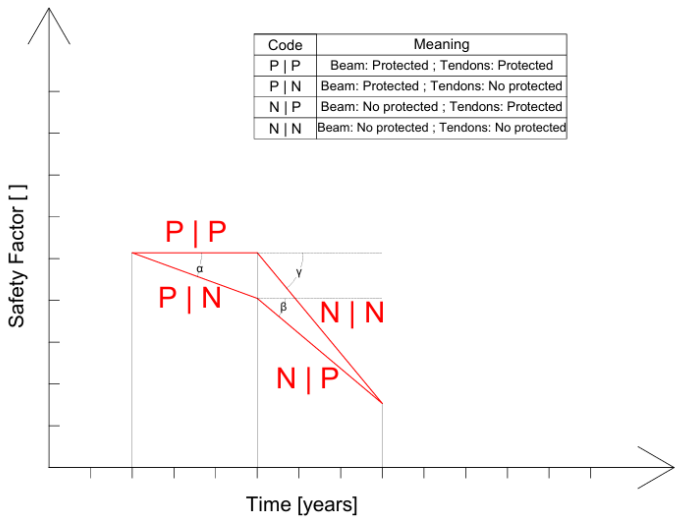

Figure 6.17. Diagram of the possible life stages of the bridge in the event of structural element replacement

This argument applies to the present case, in which the cause of failure is the beam, whose behaviour also depends on the tendons. If, instead, the tendons were the governing cause of collapse, it could be stated that performing maintenance even very close to a safety factor of 1 would not alter the lifetime of the bridge, since the behaviour of the tendons, as previously discussed, depends solely on their own condition.

This analysis further highlights that maintenance management is not always strictly linked to the structural behaviour of the system. In some cases, poorly timed maintenance may influence the performance of other structural elements, whereas in other cases such interaction does not occur. For example, in the case examined, carrying out maintenance 20 years earlier than the optimal time can reduce the overall service life of the structure by up to ten years.

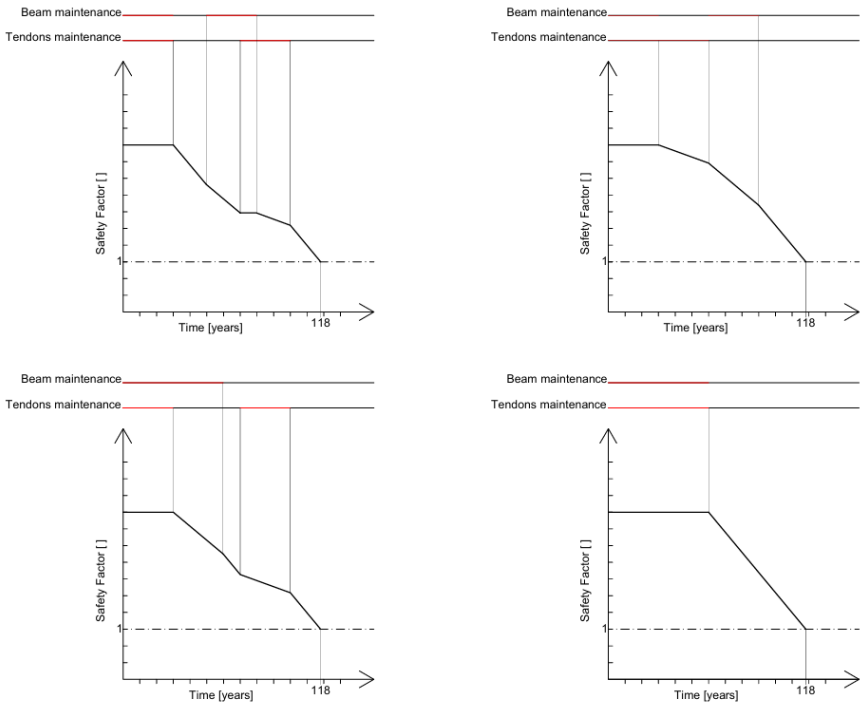

Figure 6.18. Example of the possible life stages of the bridge in the event of structural element replacement

6.0.4 Third approach: Reconstruction of structural elements

The third approach consists of performing maintenance halfway through the bridge's service life in order to slow down the progression of corrosion. When the safety factor of either of the two analysed structural elements falls below 1.01, complete maintenance is carried out and the sections of both elements are reconstructed. It is assumed that this reconstruction restores the full structural resistance of the elements. Figure 6.19 shows the envelopes of the safety factors associated with

the stresses acting on the analysed structural components. From the figure, it can be observed that the structure reaches a service life of up to 217 years, thereby extending its lifespan by 128 years.

Figures 6.20 show the analyses carried out by varying the environmental and

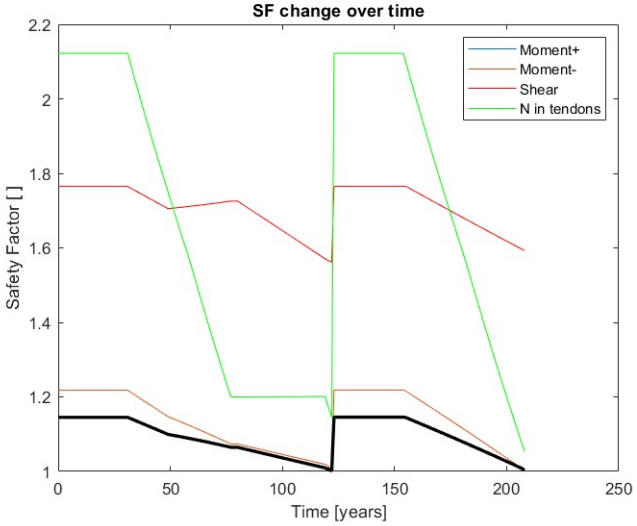

Figure 6.19. Safety Factor of the concrete bridge. Approach 3: Reconstruction of structural elements

material parameters. It can be observed that, as the service life of the structure increases and corrosion progresses, predicting the structural behaviour, and consequently making informed maintenance decisions, becomes increasingly complex. Indeed, Figure 6.20 clearly illustrates how the bundle of curves representing all analyses widens as the bridge ages, indicating a growing uncertainty in the structural response.

Furthermore, as shown in Figure 6.21, which presents the normal distributions of the years in which maintenance should be performed, the variance of these distributions increases with the service life of the structure. For example, the variance associated with maintenance on the beams at mid-life is 5.36 years, whereas the variance associated with the collapse of the structure reaches 62.93 years.

This means that the older the bridge becomes, the more frequent and detailed the inspections and monitoring activities must be.

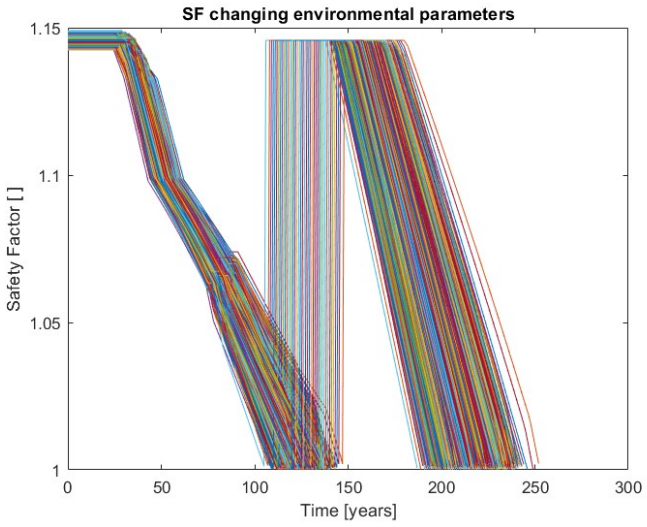

Figure 6.20. Safety Factor of the concrete bridge. Changing Parameter. Approach 3: Reconstruction of structural elements

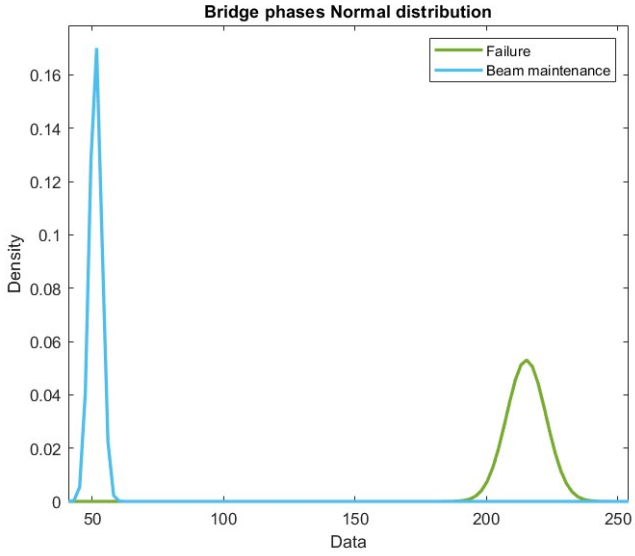

Figure 6.21. Safety Factor of the concrete bridge. Normal distributions. Approach 3: Reconstruction of structural elements

6.0.5 Cost analysis

The final step in identifying the most suitable solution is to determine which approach is the most advantageous from an economic perspective. To this end, the total cost associated with each maintenance strategy was calculated. An amortisation plan over a 20-year period was then assumed, with an annual interest rate of 4% and constant instalments; accordingly, Equation 5.3 was applied once again. Finally, the total cost, including interest, was divided by the number of years of additional service life gained through maintenance. The most cost-effective solution was identified as the one with the lowest cost per year of life extension.

Approach 2: Repainting structural elements

To carry out the repair operations, a total duration of 2 months was assumed for the beams and 1 month for the tendons and the main cable. Maintenance of the beams is scheduled at 51 years, while maintenance of the tendons and main cable is performed at 77 years. The failure of the bridge is assumed to occur at 127 years. Considering that, without maintenance, the bridge would collapse at 86 years, this maintenance approach extends the service life of the structure by 41 years.

To execute the works on the beams, it was decided to intervene on one beam at a time, allowing the other lane to remain open to traffic. The primary costs associated with the intervention are:

- Repair and restoration of missing concrete parts carried out using premixed fibre-reinforced mortar, class R3, with synthetic resins and aggregates of suitable size, for a total thickness of up to 30 mm. The work excludes formwork and any reinforcing bars required for implementation and includes the removal of damaged parts until sound concrete is reached, cleaning by manual brushing or other suitable methods, and treatment of existing reinforcing bars with converting or passivating products. The cost is measured per damaged surface area and is equal to 197.61 €/m^2.
- multidirectional scaffolding with suspended starting is used to be able to carry out the work with ease.

The secondly costs identified are:

- New Jersey type barriers for division from the other lane;
- a traffic light for traffic management;
- a construction site box and a portable toilet;

- metal nets which serve to delimit the construction site area with an attached materials storage area;
- road signs and signal lights.

The total cost for two months of work to restore the beams concrete is 46212.46 €.

The secondary maintenance costs for the tendons are very similar, although reduced to a duration of one month. In this case, the scaffolding used is a self-lifting system capable of operating at heights of up to 27 m, making it well suited for the intervention. The expected cost for this maintenance activity is 14610.48 €.

By applying this calculation, the annualized cost of extending the bridge's life using this maintenance approach can be clearly quantified. Specifically:

- Annual payment for section maintenance: 3400.41€;
- Annual payment for tendon and cable maintenance: 1075.07€
- Total cost of all maintenance work: 89,509.53€.
- Life extension achieved: 41 years

It could be say that 2183.16€ were spent to extend the life by one year.

Third approach: Reconstruction of structural elements

To carry out all the work required for this maintenance approach, the repainting operations were assumed to be identical to those described in the previous section. For the reconstruction of the section, a total duration of 4 months was considered, 2 months per carriageway, so that at least one lane remains open to traffic at all times. This strategy involves maintaining the beam with tendons to slow down corrosion at years 51 and 83. Once the bridge reaches a safety factor of 1, it is allowed to fail naturally. Under these assumptions, structural failure occurs after 217 years of service life.

The direct costs of reconstructing the sections are as follows in order of time:

- the use of scaffolding that develops above and below the roadway;
- sandblasting to remove wrinkles and clean up the reinforcement of the beam and tendons surfaces;
- Repair and restoration of missing concrete parts using fiber-reinforced premixed mortar, class R3, synthetic resins, and aggregates of suitable size, for

a total average thickness of up to 30 mm, excluding formwork and any reinforcing bars for implementation, including the removal of damaged parts until the sound concrete is reached, cleaning by manual brushing or other suitable means, including treatment of existing iron with converter or passivating products, for extensive surface interventions over 0.25 m^2: 225.42 €/ $m^{2"}$

- use of strands to reconstitute the section lost due to corrosion.
- use of reinforcement with improved adhesion to rebuild the section lost due to corrosion.

Instead, the indirect costs are very similar to those described for repainting alone, increased by 2 months. It was therefore possible to calculate the cost for repairing the load-bearing sections of the bridge, which is equal to 91063,47 €.

To calculate the depreciation of the processing cost, the formula 5.3 was used again, considering constant installments over 20 years with an annual interest rate of 4%. This resulted in an annual allocation of 6,700.61the reconstruction of the sections. Including interest, the total cost borne by the contracting party amounts to 223,521.71€ . Knowing the number of years by which the bridge's service life is extended through this maintenance strategy, it is then possible to determine the cost per additional year of service, which is equal to 1746.26 €.

Knowing these data it is possible to adopt more informed decisions, in fact with approach 2 of repainting alone the cost is 2183.16€ , which comparing it that the options described above cost almost 350€ more for each additional year of bridge life.

Chapter 7

Conclusion

The project set out to identify a predictive maintenance process capable of managing the structural elements of a bridge at a moderate cost. In the first phase, models were selected to predict the corrosion of materials such as reinforced concrete and steel. Although numerous models exist in the literature, the main challenge lies in choosing those supported by data collected under a wide range of environmental conditions. For carbon steel, this task was facilitated by databases such as ISOCORRAG, ICP/UNECE, and MICAT, which compile data from steel bridges across Europe. For reinforced concrete, the process was more complex, as many existing models are based on specific laboratory tests or on structures located in particular environments. Nevertheless, it was possible to identify models that offer a reasonable degree of reliability.

Once the degradation models were selected, a case study was defined to provide a realistic context for their application. By placing the bridge in a specific location, the relevant environmental parameters could be determined with relative ease. In Piedmont, and in Italy more broadly, such data are readily available through regional environmental protection agencies. A structural model was also chosen that allows for straightforward modification of geometric characteristics to account for corrosion-induced section loss. Three maintenance approaches were ultimately selected from among many possible strategies to extend the service life of the bridge. Varying the environmental parameters, and therefore the rate of degradation, was essential to account for potential fluctuations in section loss due to environmental variability and uncertainties in the adopted models.

The results demonstrate that the original objective of the project was achieved: a predictive maintenance process was identified that accounts for both time-dependent corrosion and the evolving structural behaviour of the bridge. For example, Section 5.0.3 highlighted the importance of structural analysis by showing that increasing

tendon protection can paradoxically reduce the overall service life of the bridge. This occurs because maintaining high tendon stiffness while beam stiffness decreases may lead to failure under excessive negative bending moments. A similar principle was observed for tendon maintenance. Section 6.0.3 further showed that, provided the period during which the structure remains protected is fully exploited, the exact timing of maintenance on different structural elements is not critical. In such cases, the principle of overlapping effects can be applied at different stages of the bridge's life, ensuring optimal use of protective interventions.

Implementing this type of predictive maintenance enables more efficient planning of interventions. Knowing the normal distribution of expected maintenance periods allows decision-makers to determine the optimal timing of interventions while balancing structural safety and long-term cost management. At a relatively low cost, this project provides authorities with a tool to support more informed, data-driven maintenance decisions.

The project does, however, include several simplifications that were necessary for the scope of this thesis. The first concerns the degradation models, which, particularly for reinforced concrete, do not perfectly represent the behaviour of the materials in the case study. For instance, the actual steel composition may differ, or the presence of cracks in the concrete could accelerate carbonation. The second simplification relates to the structural model: the main cable was assumed to have no structural effect. While acceptable for the purposes of this study, this assumption introduces some error in the structural response. A third simplification concerns the modelling of concrete strength, which was always assumed to correspond to field-3 failure. This assumption is reasonable because the design aimed to resist in field 3; thus, small increases in moment would still lead to maximum deformations in both steel and concrete. Finally, the project focuses exclusively on failure due to the ultimate limit state associated with corrosion, without considering the effects of load cycles over the bridge's lifetime.

There are several opportunities to improve and expand this work. Future developments could include the creation of degradation models tailored to specific materials or environmental conditions. The structural analysis could be enhanced by generalising the MATLAB code to handle any type of suspension bridge with multiple spans, or by incorporating finite element models to account for the behaviour of the main cable. Additional maintenance strategies could be explored, including the use of innovative materials. The cost analysis could also be refined to optimise maintenance financing methods. Moreover, future studies could consider all limit states defined by Italian or European construction codes.

While the project successfully achieved its objectives, there remains significant potential for improvement and generalisation. With appropriate adaptations, the predictive maintenance framework developed for cable-supported bridges could also be applied to the maintenance management of other bridge typologies.

Bibliography

[1] Fathi Habashi. History of corrosion research. *ResearchGate*, 2003.

[2] Khairy Ahmed Helmy Kobbacy and DN Prabhakar Murthy. *Complex system maintenance handbook*. Springer Science & Business Media, 2008.

[3] R Keith Mobley. *An introduction to predictive maintenance*. Elsevier, 2002.

[4] Hashem M Hashemian. State-of-the-art predictive maintenance techniques. *IEEE Transactions on Instrumentation and measurement*, 60(1):226–236, 2010.

[5] Abdoul S Bah, Yan Zhang, Kotaro Sasai, David Conciatori, Luc Chouinard, Nicolas Zufferey, Gabriel J Power, Thomas Sanchez, and Xuande Chen. Bridge service life and impact of maintenance events on the structural state index. *Case Studies in Construction Materials*, page e04766, 2025.

[6] Valerio De Biag; Lorenzo Casasso; Marco Domaneschi; Bernardino Chiaia. Predictive maintenance of cable supported bridges: Integrating damage evolution, cost analysis, and data-driven decision support. In *IABSE Symposium*, 2026.

[7] Gaurav Somani. A comparative study on t girder bridge deck using grillage analogy and finite element method. *International Journal of Engineering Research Technology*, 2021.

[8] Paolo Clemente. L'evoluzione dei ponti: materiali e schemi strutturali. *Ingenio*, 2018.

[9] P.E Najib Gerges, Ph.D. The basic types of bridges. *CEDengineering.com*, 2022.

[10] Paolo Castaldo. L'evoluzione costruttiva dei ponti. Laboratorio Tematico 2.

[11] M. Haskins. What is a girder bridge? *https://erkrishneelram.wordpress.com/2015/01/21/what-is-a-girder-bridge/*, 2015.

[12] Bridge Design Lectures. Superstructure / girder bridges. Chair of Concrete Structures and Bridge Design;ETH Zürich.

[13] KENNETH TIOTSOP. Redundancy and resilience of arch bridges. case study of the polcevera railway arch bridge in genoa, italy. 2022.

[14] Qianrui Niu. Review on the development of truss bridges. *Academic journal of science and technology*, 2022.

[15] Wikipedia. Bridge.

[16] CICLOPEDONALE SUL FIUME Claudio Migliorini. Progettazione di un ponte strallato. 2016.

[17] Marco Petrangeli et al. Grandi strutture sospese. In *XXI SECOLO. Gli Spazi e le arti*, volume 4, pages 315–326. Istituto della Enciclopedia Italiana-Treccani, 2010.

[18] Bharat Singh, V Revathi, Amit Dutt, Rallabandi Venkata Santoshi Saraswati Swetha Nagini, Pramod Kumar, Hazim Y Saeed, and M Sundeep. Suspension bridges versus cable-stretched bridges: a comparison of structural behaviour and performance. In *E3S Web of Conferences*, volume 552, page 01112. EDP Sciences, 2024.

[19] *LVH APA; Manuale del calcestruzzo.*

[20] New Millenium. 46,154; u.s bridges need repairing. stay-in-place bridge deck forming systems can help get them done quicker and safer.

[21] Prof.Ing. Valerio De Biagi. Tipologie di difetti presenti sui viadotti e loro eziologia. *SOCIETÀ ITALIANA PER IL TRAFORO DEL GRAN SAN BERNARDO RACCORDO AUTOSTRADALE GRAN SAN BERNARDO*, 2023.

[22] Tomas Ekström. *Leaching of concrete: the leaching process and its effects*, volume 1020. Lund University, 2003.

[23] Y Rivela and L Sgambi. Modellazione dei processi di degrado. *Handling Exceptions in Structural Engineering, Rome*, 2010.

[24] Xinhao Wang, Qiuwei Yang, Xi Peng, and Fengjiang Qin. A review of concrete carbonation depth evaluation models. *Coatings*, 14(4):386, 2024.

[25] Kaijian Zhang and Jianzhuang Xiao. Prediction model of carbonation depth for recycled aggregate concrete. *Cement and Concrete Composites*, 88:86–99, 2018.

[26] RV Silva, A Silva, R Neves, and J De Brito. Statistical modeling of carbonation in concrete incorporating recycled aggregates. *Journal of Materials in Civil Engineering*, 28(1):04015082, 2016.

[27] Lech Czarnecki and Piotr Woyciechowski. Concrete carbonation as a limited process and its relevance to concrete cover thickness. *ACI Materials Journal*, 109(3):275, 2012.

[28] CEB-FIB. *MODEL CODE 1990*. Thomas Telford, 1990.

[29] Matteo Felitti. Penetrazione dei cloruri nelle strutture in calcestruzzo armato. *FIBRE NET*, 2022.

[30] Federico Liotta. Corrosione nelle strutture in calcestruzzo: effetti, modellazione, prevenzione e manutenzione. 2022.

[31] Luigi Di Sarno, Armin Majidian, and George Karagiannakis. The effect of atmospheric corrosion on steel structures: A state-of-the-art and case-study. *Buildings*, 11(12):571, 2021.

[32] Charis Apostolopoulos and Konstantinos Koulouris. Corrosion effect on bond loss between steel and concrete. In *Structural Integrity and Failure*. IntechOpen, 2020.

[33] E Chen, Carlos G Berrocal, Ingemar Löfgren, and Karin Lundgren. Correlation between concrete cracks and corrosion characteristics of steel reinforcement in pre-cracked plain and fibre-reinforced concrete beams. *Materials and Structures*, 53(2):33, 2020.

[34] Kerman Vázquez, Raúl Rubén Rodríguez, and M Dolores Esteban. Corrosion prediction models in the reinforcement of concrete structures of offshore wind farms. *Journal of Marine Science and Engineering*, 10(2):185, 2022.

[35] Dawei Zhang, Yu Zeng, Mingshan Fang, and Weiliang Jin. Service life prediction of precast concrete structures exposed to chloride environment. *Advances in Civil Engineering*, 2019(1):3216328, 2019.

[36] Ahmed Merah. Concrete anti-carbonation coatings: a review. *Journal of Adhesion Science and Technology*, 35(4):337–356, 2021.

[37] Peter Thissen, Andreas Bogner, and Frank Dehn. Surface treatments on concrete: An overview on organic, inorganic and nano-based coatings and an outlook about surface modification by rare-earth oxides. *RSC Sustainability*, 2(8):2092–2124, 2024.

[38] Regione Piemonte. Prezzario regione piemonte. *https://www.servizi.piemonte.it*, 2025.

[39] Yongqin Liang and Licheng Wang. Effect of water-to-cement ratio on service life of reinforced concrete structures in chloride environment. *Structural Concrete*, 22(5):2748–2760, 2021.

[40] Tao Fan, Yongchang Wu, Mingda Yang, Peng Xu, Yongqing Li, Laifa Wang, and Huaxin Chen. Attenuation law of performance of concrete anti-corrosion coating under long-term salt corrosion. *Coatings*, 14(10):1249, 2024.

[41] Jorge E. Pagán-Ortiz. Multiple corrosion-protection systems for reinforced concrete bridge components. Technical report, U.S. Departement of transportation, 2011.

[42] Association Française de Génie Civil. *Rehabilitation Guide – Repair of Reinforced Concrete Structures (English version)*. AFGC, 2007.

[43] ACRP. Reinforcement repair and protection technologies. In *The Guide about Technologies of repair and reinforcement of concrete structures*, 2024.

[44] *Manual on Service Life of Corrosion-Damaged Reinforced Concrete Bridge Superstructure Elements. NCHRP Report 558, Transportation Research Board, Washington, D.C.*

[45] *Guideline for Surface Preparation for the Repair of Deteriorated Concrete Resulting from Reinforcing Steel Corrosion (ICRI 310.1R-2008). International Concrete Repair Institute, Chicago, USA.*

[46] Ali Jahami and Camille A Issa. An updated review on the effect of cfrp on flexural performance of reinforced concrete beams. *International Journal of Concrete Structures and Materials*, 18(1):14, 2024.

[47] Sudeep Adhikari. Mechanical properties and flexural applications of basalt fiber reinforced polymer (bfrp) bars. Master's thesis, University of Akron, 2009.

[48] Belén Chico, Daniel De la Fuente, Iván Díaz, Joaquín Simancas, and Manuel Morcillo. Annual atmospheric corrosion of carbon steel worldwide. an integration of isocorrag, icp/unece and micat databases. *Materials*, 10(6):601, 2017.

[49] FL Lipfert and M Benarie. A general corrosion function in terms of atmospheric pollutant concentrations and rain ph. *Atmospheric Environment*, 20(10):1947–1958, 1986.

[50] Dawn E Klinesmith, Richard H McCuen, and Pedro Albrecht. Effect of environmental conditions on corrosion rates. *Journal of Materials in Civil Engineering*, 19(2):121–129, 2007.

[51] https://galvanizeit.org/. American galvanizers association.

[52] *https://www.abate.it/trattamenti-superficiali/zincatura-metallizzazione.html*.

[53] Weiliang Ni, Peng Li, Yajun Zhu, Zhigang Di, Liangliang Guo, and Yunqi Liu. Comparative study of anti-corrosion properties and lifespan prediction model for inorganic zinc-rich coating and thermal-spray zinc coating. *Coatings*, 12(4):505, 2022.

[54] Rob B Polder, Greet Leegwater, Daniël Worm, and Wim Courage. Service life and life cycle cost modelling of cathodic protection systems for concrete structures. *Cement and Concrete Composites*, 47:69–74, 2014.

[55] *Guidelines for Field Repairs and Retrofits of Steel Bridges. AASHTO/NSBA STEEL BRIDGE COLLABORATION*, G14.2—2023.

[56] Jean-Pierre Michel Chacar. Design of cable systems for cable suspended bridges. Master's thesis, Massachusetts Institute of Technology, 2001.

[57] Efe Karanci and Raimondo Betti. Modeling corrosion in suspension bridge main cables. i: Annual corrosion rate. *Journal of Bridge Engineering*, 23(6):04018025, 2018.

[58] Kazuhiko Furuya, Makoto Kitagawa, Shun-ichi Nakamura, and Keita Suzumura. Corrosion mechanism and protection methods for suspension bridge cables. *Structural engineering international*, 10(3):189–193, 2000.

[59] Keita Suzumura and Shun-ichi Nakamura. Environmental factors affecting corrosion of galvanized steel wires. *Journal of materials in civil engineering*, 16(1):1–7, 2004.

[60] Kazuhiko Furuya, Makoto Kitagawa, Shun-ichi Nakamura, and Keita Suzumura. Corrosion mechanism and protection methods for suspension bridge cables. *Structural engineering international*, 10(3):189–193, 2000.

[61] Tatjana Grigorjeva, Algirdas Juozapaitis, and Zenonas Kamaitis. Static analysis and simplified design of suspension bridges having various rigidity of cables. *Journal of Civil Engineering and Management*, 16(3):363–371, 2010.

[62] *NTC 2018; Capitolo 5. Ponti*.

[63] *ARPA Piemonte; https://www.arpa.piemonte.it/territorio/torino*.

[64] Uno sguardo all'aria. *ARPA*, 2024.

[65] *BS EN ISO 9223:2012; Corrosion of metals and alloys — Corrosivity of atmospheres — Classification, determination and estimation.*

[66] *OPPO; https://www.oppo.it/.*

[67] Edoardo COSENZA. Approfondimento delle basi concettuali e valutazioni operative per le verifiche disicurezza accurate. Università di Napoli Federico II.